

The Relevance of Measurement Systems Analysis

A Procter & Gamble Case Study on
MSA Methodology and Applications

DATE

**OCTOBER
10 AND 12**

TIME

**16:00 CET,
10 am EST**



**CHRISTIAN
NEU**

Scientist
Procter & Gamble



**JERRY
FISH**

Systems Engineer
JMP



**JASON
WIGGINS**

Senior Systems
Engineer
JMP

[Register now](#)

Hot Sheet Metal Forming Strategies for High-Strength Aluminum Alloys: A Review—Fundamentals and Applications

Emad Scharifi,* Victoria A. Yardley, Ursula Weidig, Damian Szegda, Jianguo Lin, and Kurt Steinhoff

In the past decade, aluminum alloys have become important structural materials in the automotive industry, thanks to their low density, high strength, high fracture toughness, and good fatigue performance. However, an important limitation of aluminum alloys is their poor formability at room temperature; as a result, numerous studies have been conducted with the aim of developing forming techniques to overcome this and facilitate the forming of more complex-shaped components. Following an overview on the metallurgical background of aluminum alloys, this article reviews recent developments in forming processes for aluminum alloys. The focus is on process variants at room temperature and at higher temperatures and on a new hot forming technique promising considerable improvements in formability. This review summarizes the influence of different process parameters on microstructures and mechanical properties. Particular emphasis is given to process design and to the underlying microstructural phenomena governing the strengthening mechanisms.


1. Introduction

The international push toward reducing CO₂ emissions, which is increasingly enshrined in legal regulations, has led to a growing

E. Scharifi, U. Weidig, K. Steinhoff
Metal Forming Technology
University of Kassel
Kurt-Wolters-Strasse 3, Kassel 34125, Germany
E-mail: emad.scharifi@uni-kassel.de

V. A. Yardley, J. Lin
Department of Mechanical Engineering
Imperial College London
London SW7 2AZ, UK

D. Szegda
Technology - Research & Development
Impression Technologies Limited
London, UK

 The ORCID identification number(s) for the author(s) of this article can be found under <https://doi.org/10.1002/adem.202300141>.

© 2023 The Authors. Advanced Engineering Materials published by Wiley-VCH GmbH. This is an open access article under the terms of the Creative Commons Attribution-NonCommercial-NoDerivs License, which permits use and distribution in any medium, provided the original work is properly cited, the use is non-commercial and no modifications or adaptations are made.

DOI: 10.1002/adem.202300141

demand for lightweighting across the automotive industry, especially for electric vehicles.^[1–4] This requires the development of sheet materials that have a higher strength-to-weight ratio than the steels currently used, and that can be produced at reasonable cost. Aluminum alloys, which are already used extensively in the aerospace sector, have been identified as a replacement material because of their excellent combination of properties^[5,6] and have already been used in production vehicles for the luxury market.^[7] The sheet forming process requires a high dynamic force and consists of several deformation steps with elaborate strain paths leading to effects such as springback (i.e., elastic recovery resulting in deviation from the desired shape after release of the work-piece), local thinning, and the nucleation

and propagation of damage.^[8–11] These effects occur even at low strains during forming at room temperature (RT),^[12] so these alloys are considered to have low room-temperature formability. In contrast, forming at elevated temperatures both increases formability and decreases springback, allowing the design of more complex-shaped part geometries, but often entails an undesired reduction in mechanical strength.^[13] For this reason, a variety of new approaches to sheet metal forming, and especially to the hot forming of high-strength aluminum alloys, have been developed to simultaneously overcome formability limits, enabling the forming of more complex-shaped components and to improve final mechanical properties. The common element of all these strategies is the application of thermally activated softening mechanisms during hot forming and of strengthening mechanisms during aging, particularly of precipitation hardening (PH) in heat-treatable aluminum alloys. The present article is devoted mainly to a review of recent research and development on hot sheet metal forming strategies for high-strength aluminum alloys for use in the automotive industry. Section 2 presents the metallurgical basis for understanding the relationship between process parameters and mechanical and physical properties, namely, information on alloy classifications and the fundamental microstructural phenomena governing the strengthening mechanisms. Section 3 focuses on recently developed cold, warm, and hot forming techniques, mainly considering the effect of process parameters such as heating rate, solution heat treatment temperature and

cooling rate, on the material formability behavior, flow characteristics, and final mechanical properties. The spotlight in Section 4 is on a new thermomechanical method, namely, solution heat treatment forming and in-die quench (HFQ), which was first proposed by Lin et al.,^[14,15] and is a registered trademark of Impression Technologies Limited. The final part of the article presents summary and conclusions.

2. Aluminum and Aluminum Alloys

Commercially pure aluminum (99% Al or greater) has good thermal and electrical conductivity, enabling its use as a functional material in applications involving heat transfer between different contact surfaces and/or conduction of electricity. Its low melting temperature means that less energy is required for thermally activated processes, such as casting or hot forming, than is the case for steel processing. Its low strength properties (yield strength [YS] of 20 MPa and ultimate tensile strength [UTS] of 80 MPa.^[16]) preclude its use in structural applications. However, it has long been known that aluminum can be transformed into a technically relevant structural material by alloying with elements such as copper, lithium, magnesium, silicon, or zinc.^[16]

2.1. Classification of Aluminum Alloys

Depending on the chemical composition and the application field, aluminum alloys are divided into cast and wrought alloys.

Table 1. Classification of wrought alloys, with main properties, applications, and hardenability.

Wrought alloy designation	Major components	Main properties and applications	Hardenability properties
1xxx	Al (>99%)	Very high corrosion resistance. High thermal and electrical conductivity, poor mechanical properties.	Nonhardenable
2xxx	Al–Cu	Requires heat treatment to obtain optimum properties. Used widely in aerospace industry. Structures and parts for elevated-temperature use.	Age-hardenable
3xxx	Al–Mn	Good formability, moderate strength.	Solution hardening
4xxx	Al–Si	Used in welding wire and as brazing alloys due to low melting point.	Nonhardenable
5xxx	Al–Mg	Moderate-to-high strength, good welding characteristics, and good resistance to corrosion in marine and aerospace environments.	Solution hardening
6xxx	Al–Mg–Si	Good formability and corrosion resistance, medium strength.	Age hardenable
7xxx	Al–Zn–Mg–(Cu)	Very high strength, prone to fatigue.	Age hardenable
8xxx	Al–Li–Cu–Mg	Improved elevated-temperature performance, medium strength.	Age hardenable

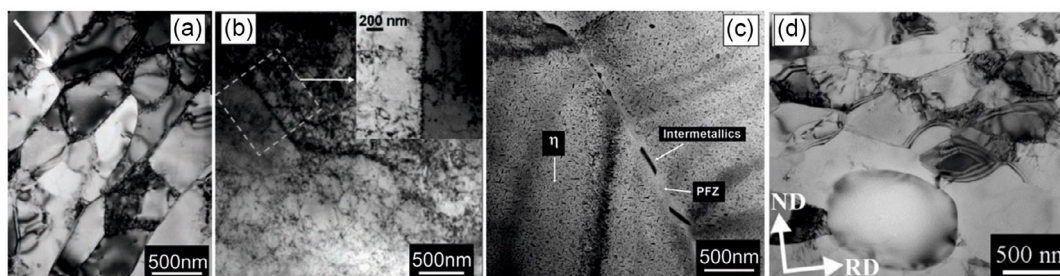


Figure 1. TEM micrographs of pure aluminum and selected aluminum alloys: a) pure aluminum. Reproduced with permission.^[202] Copyright 2011, Elsevier. b) nonheat-treatable AA5754 showing dislocation walls. Reproduced with permission.^[203] Copyright 2019, MDPI. c) heat-treatable AA7050 including second-phase particles. Reproduced with permission.^[204] Copyright 2016, SciELO and d) heat-treatable AA8006.

Cast alloys with high silicon content are used for castings of, for example, transmission housings or pistons, while wrought alloys are found in bulk and sheet metal forming. Wrought alloys (Table 1) are further divided into non-heat-treatable and heat-treatable materials. Non-heat-treatable alloys derive their mechanical properties purely from the alloying elements and the forming process, whereas heat-treatable (also known as age-hardenable) alloys require specific heat treatment to develop their maximum strength.^[17] The highest mechanical strength of a heat-treatable alloy is found in its peak-hardened state, commonly designated as the T6 condition (solution heat treated, water quenched, and artificially aged to peak strength).

Transmission electron microscopy (TEM) images of pure aluminum and of selected aluminum alloys are shown in Figure 1. In the pure aluminum (Figure 1a) and the non-heat-treatable alloy, (Figure 1b, a high dislocation density and equiaxed subgrains are observed, whereas the heat-treatable aluminum alloys, Figure 1c,d), show small precipitates homogeneously distributed inside the grains.

2.2. Strengthening Mechanisms in Aluminum Alloys

The strength of polycrystalline metallic materials, including aluminum alloys, is directly related to their resistance to plastic deformation; this, in turn, depends on the ability of the microstructure to resist the motion of dislocations (slip).^[18,19] There are several different microstructural mechanisms by

which slip is hindered and the shear stress required to initiate and maintain plastic flow increases; these mechanisms can be exploited to strengthen the material. In aluminum alloys, four major mechanisms are known: solid-solution strengthening (SSS), grain boundary (GB) strengthening, strengthening via dislocation–dislocation interactions (strain or work hardening, WH), and PH or PH. The mechanisms contribute to the overall YS of the alloy σ according to

$$\sigma = \sigma_0 + \sigma_{SSS} + \sigma_{GB} + \sigma_{WH} + \sigma_{PH} \quad (1)$$

where σ_0 is the frictional stress of the aluminum lattice (≈ 35 MPa for pure aluminum^[20]), and σ_{SSS} , σ_{GB} , σ_{WH} , and σ_{PH} are the strength contributions from SSS, GB strengthening, strain hardening, and PH, respectively.

2.3. Solid-Solution Strengthening

According to dislocation theory, solid-solution hardening is attributed to an increase in the critical resolved shear stress resulting from the presence of foreign atoms on interstitial or substitutional positions in the crystal lattice. This increase in strength is caused by the interaction of the stress fields around solute atoms with the stress fields around dislocations. A solute atom can cause a compressive strain field (if the solute atom is substitutional and larger than the matrix atoms or if it is in an interstitial position) or a tensile strain field (if the solute atom is substitutional and smaller than the matrix atoms). The interaction of these strain fields with the compressive and tensile strain fields around dislocations allows the dislocations to adopt a lower-energy configuration; energy input is required to dislodge the dislocation from this configuration. A mismatch in elastic modulus between the solute and matrix atoms can reinforce or weaken this pinning effect. All aluminum alloys derive their intrinsic strength through this mechanism. The strength depends strongly on the chemical nature of the alloying elements themselves, their concentration, and their configuration within the crystal lattice (Figure 2). It has been shown that an almost linear correlation exists between the mechanical strength and the amount of magnesium (Mg), and that the same is the case for manganese

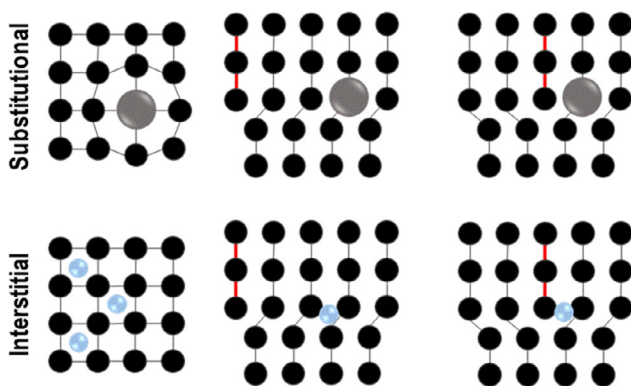


Figure 2. Solid-solution hardening: Introducing foreign atoms onto interstitial or substitutional positions in the crystal lattice hinders dislocation motion by inducing opposing elastic lattice strains and other mutual reactions. The degree of strengthening depends on the shear stress required to move dislocations past these atoms.

(Mn), for a large number of commercial aluminum alloys.^[21] The strength contribution from dissolved alloying elements can be expressed as follows for the example of AA7075.^[22]

$$\sigma_{SSS} = MA_{Zn} C_{Zn}^{2/3} + MA_{Mg} C_{Mg}^{2/3} \quad (2)$$

where M is the Taylor factor, A_{Zn} and A_{Mg} are strength coefficients, and C_{Zn} and C_{Mg} are the concentrations of Zn and Mg in solid solution in the Al matrix. Note that these concentrations C_{Zn} and C_{Mg} are not the same as the overall concentration of the corresponding element in the alloy unless all precipitate and dispersoid phases are completely dissolved.

2.4. Grain Boundary Strengthening

The interfaces between neighboring grains act as very strong obstacles to the motion of dislocations through the lattice due to differences in grain orientation (Figure 3). Therefore, GB strengthening constitutes another mechanism by which the strength of aluminum alloys may be enhanced. Increasing the total area of GBs in the material, i.e., reducing the grain size, through grain refinement treatments^[23] raises the critical shear stress associated with the GB strengthening effect. The contribution to YS σ_{GB} from GBs is related to the average grain size d according to the Hall–Petch relationship.^[24]

$$\sigma_{GB} = \frac{k_y}{\sqrt{d}} \quad (3)$$

Here, k_y is a strengthening coefficient.^[24]

The effect of grain size distribution is investigated on AA8021 in another study^[25] on the mechanical properties and deformation behavior using tensile tests and Erichsen cupping test, which are then characterized using different electron microscopic techniques. It is shown that with increasing the grain size, the yield and ultimate tensile strength as well as the Erichsen values decrease, which is related to the ratio of free surface to

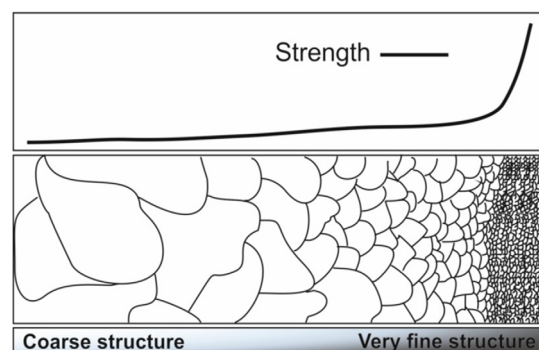


Figure 3. GB strengthening and grain refinement, from coarse to fine microstructure. GBs in polycrystalline microstructures impede dislocation movement due to grain orientation differences. Decreasing the grain size through thermomechanical treatment and microalloying^[206] increases the total area of boundaries, resulting in strengthening of the material. This strengthening method is used in both heat-treatable and nonheat-treatable aluminum alloys.^[207]

volume of the grains and the decrease of GB number existing in the microstructure.

2.5. Work Hardening

Dislocation strengthening, also known as work or strain hardening, is the consequence of irreversible deformation usually occurring below the recrystallization temperature and leading to the multiplication of dislocations and a consequent dramatic increase in their density (Figure 4).^[18] The dislocations accumulate, and their stress fields interact with each other to an increasing extent, during their sliding movement. The resulting shear strength contribution from dislocation interactions, τ , can be obtained from the shear modulus for aluminum G , the dislocation density ρ_{\perp} , and the magnitude of the Burgers vector b , according to the following equation.

$$\tau = Gab\sqrt{\rho_{\perp}} \quad (4)$$

where α is a constant and $\alpha < 1$ represents dislocations that can be considered as penetrable obstacles.^[26] In precipitate-free aluminum alloys, the evolution of the density of statically stored dislocations ρ_s is described by the Kocks–Mecking–Estrin formulation as follows.

$$\frac{\partial \rho_s}{\partial \varepsilon_p} = M(k_1\sqrt{\rho_s} - k_2\rho_s) \quad (5)$$

Here, M is the Taylor factor, ε_p the plastic strain, k_1 is related to the rate of dislocation storage, and k_2 to the rate of dynamic recovery during plastic deformation.^[27,28] The interactions between intersecting dislocations create an increasing density of immobile dislocations. This strengthening mechanism is very effective in cold-forming processes such as extrusion, rolling, or deep drawing. It is mostly used in nonheat-treatable aluminum alloys to increase the strength in the final forming step,^[29] but also affects the final mechanical properties via thermally activated mechanisms such as dynamic recrystallization and dynamic recovery as well as second-phase precipitation in heat-treatable alloys, for example, Al–Zn–Mg 7xxx alloys, with the dominant effects and their kinetics depending on the forming temperature and deformation rate.^[30]

Dislocations can be generated at GBs, elastically distorted interfaces between lattice matrix and particles, and at free surfaces. The accumulated total local stress in excess of the YS causes

the formation of dislocations by homogenous nucleation via Frank–Read source.^[18,31] This leads to the movement of dislocations along their slip planes and their interaction with and hindering of each other via pinning effects and cutting of dislocation lines. Frank-Read sources, such as second phases within the grain structure, can also act as barriers to dislocations impeding their movement. With increasing applied stress, dislocations increasingly attempt to glide along the slip plane, but only unpinned dislocation segments are capable of movement and the pinned segments remain stationary.^[18,31] This phenomenon with increasing stress, causes the dislocations to bend and form loops around the secondary phases. If the dislocation loop touches itself, a new dislocation is generated; this can move away from the pinned dislocation, whereas the pinned dislocation remains trapped around the second-phase particle. Hence, during plastic deformation, the generation of new dislocations is continuously repeated via the process described, leading to an enormous increase in dislocation density.^[18,31,32]

2.6. Precipitation or Age Hardening

The most effective and important strengthening mechanism in heat-treatable wrought aluminum alloys is PH or. This is induced via special heat treatments consisting of solution annealing, quenching, and subsequent aging. The presence of nanoscopic second-phase precipitate particles within aluminum grains causes distortion of the crystal lattice. The associated stress fields interact with moving dislocations and impede their motion. Depending on the size of the precipitates as well as the distance between them, dislocations moving under external stress may overcome them either by cutting (Kelly–Fine mechanism) or bowing (Orowan mechanism), Figure 5.^[18,33] The shear stress required to overcome the obstacles gives rise to an increase in strength whichever mechanism is in operation. The precipitate size, number density, and distance between adjacent precipitates play a decisive role in which mechanism predominates. Fine precipitates with coherent or partially coherent interfaces with the matrix predominantly undergo cutting according to the Kelly–Fine mechanism, while coarse, incoherent precipitates are bypassed according to the Orowan bowing mechanism, which leaves a dislocation loop around the particle.^[34,35] In the case of fine, coherent precipitates, the magnitude of the shear stress $\Delta\tau_{p, \text{cutting}}$ required for the cutting of the precipitates by dislocations depends on the precipitate radius r .^[35,36]

$$\Delta\tau_{p, \text{cutting}} \approx k\sqrt{\frac{fr}{b}} \quad (6)$$

Here, k is a material constant and f is the volume fraction of the precipitates.

For larger precipitates, Orowan bowing predominates, and the precipitate spacing L_p determines the stress required for the obstacle to be overcome.

$$\Delta\tau_{p, \text{bowing}} \approx \frac{Gb}{L_p - 2r} \approx \frac{Gb\sqrt{f}}{2r}, \quad r \ll L_p \quad (7)$$

where G is the shear modulus and b is the magnitude of the Burgers vector.^[36]

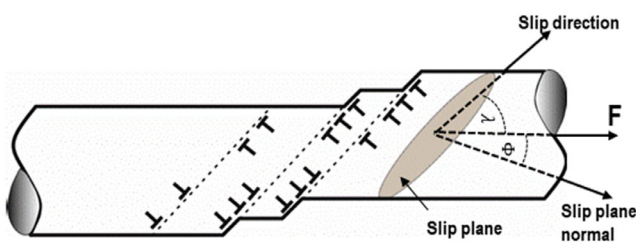


Figure 4. Dislocation strengthening (work hardening). Irreversible (plastic) deformation of aluminum at temperatures below the recrystallization temperature increases the dislocation density^[208] through dislocation multiplication. Mutual interactions between dislocations cause strengthening (strain hardening).^[209]

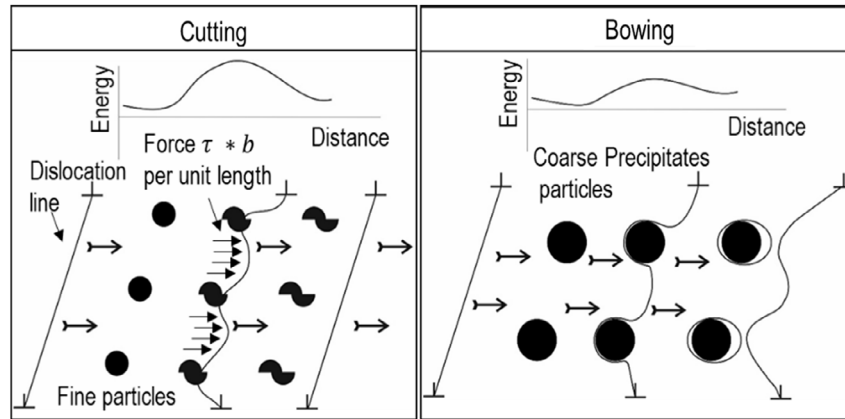


Figure 5. PH. Nanoscale precipitates of second phases, which nucleate and grow during controlled heat treatments and give the most pronounced strengthening of all microstructural mechanisms. Depending on the size and spacing of the precipitates, the moving dislocations overcome them either by cutting (Kelly–Fine mechanism) or bowing (Orowan mechanism);^[18] both mechanisms require additional stress which leads to the increased strength.

The maximum strength is obtained at an intermediate precipitate radius r_{crit} , which represents the transition from the Kelly–Fine to the Orowan mechanism. The extent of the resulting strengthening effect in precipitation-hardenable aluminum alloys is thus associated directly with the precipitate size and distribution. The terminology T6 is used to designate the condition in which an age-hardenable aluminum has attained its maximum hardness; this is achieved by a controlled heat treatment known as artificial aging, usually at temperatures of around 100–200 °C. However, precipitation can also occur if age-hardenable alloys are left at room temperature for sufficient time. This process is called natural aging and results in a condition designated T4. **Table 2** gives the precipitation sequences in age-hardenable aluminum alloys.

The PH process in hardenable aluminum alloys is governed by the different precipitation sequences appearing during natural aging at room temperature or artificial aging at moderate temperatures. The different precipitation sequences are responsible for the changes in crystallographic structure of the particles nucleated after fast cooling from solution heat treatment to give a supersaturated condition. Taking the 7000 precipitation-hardenable aluminum alloys as an example from **Table 2**, the first precipitates appearing after the formation of very small atomic clusters are GP zones, which can be detected only by high-resolution transmission microscopy techniques.^[37] These zones usually nucleate during natural aging at room temperature

Table 2. Precipitation sequences and stages of decomposition after fast cooling from solution heat treatment in heat-treatable (age-hardenable) aluminum alloys. A variety of different precipitate phases formed temperatures below solvus depending on the chemical composition of the precipitation-hardenable aluminum alloy.

Alloy series	Main alloying elements	Precipitation sequence
2xxx	Al, Cu–(Mg)	GP → θ'' → θ' (CuAl ₂)
6xxx	Al, Mg, Si	GP → β'' → β' → β (Mg ₂ Si)
7xxx	Al, Zn, Mg–(Cu)	GP → η' → η (MgZn ₂)
8xxx	Al, Li	δ' (Al ₃ Li) → δ (AlLi)

or in the early stages of artificial aging treatment at moderate temperatures, as shown in **Table 2**. In the precipitation-hardenable alloy AA7050, for example, two different types of GP zones are reported.^[38] It has been shown that the GP I zones are fully coherent with the aluminum matrix and the GP II zones are characterized by zinc-rich layers on the {111} aluminum plane. These zones are the precursors of η' precipitates for 7000 series precipitation-hardenable aluminum alloys.^[39] The η' phase is the main precipitate phase contributing to the strength of 7000-series alloys. However, the exact nucleation and growth mechanisms of these nanoscopic particles are still debated due to their extremely small size in the initial stages of nucleation and growth. Different scenarios for the formation of η' precipitates have been proposed in the literature. While in other studies^[40,41] the transformation of small GP I zones into η' phase is stated to be the dominant mechanism for the formation of η' phase, in other studies,^[42,43] GP II zones are reported to be the main nucleation sites for the metastable η' precipitates. The platelet-shaped η' phases are reported to have a hexagonal crystal structure with lattice parameters of $a = b = 0.496$ nm and $c = 1.402$ nm ($\approx 6 \times$ the unit cell dimension of Al).^[39,43–45] Hence, the crystallographic orientation relationships are reported in other studies^[39,43,46,47] to be as follows: $[1010]_{\eta'} // [110]_{Al}$ and $(0001)_{\eta'} // (111)_{Al}$; $(0001)_{\eta'} // (111)_{Al}$ and $[1010]_{\eta'} // [110]_{Al}$; $(0001)_{\eta'} // (111)_{Al}$ and $[1010]_{\eta'} // [110]_{Al}$; $(0001)_{\eta'} // (111)_{Al}$ and $[1010]_{\eta'} // [110]_{Al}$.^[39] In the next steps of the sequence, the GP zones fully transform with sufficient time and temperature into metastable η' phase and eventually these are replaced by stable η precipitates, as shown in **Table 2**.

3. Forming Strategies to Overcome the Forming Limit of Aluminum Alloys

Sheet metal forming processes for thin-walled aluminum alloys require different thermomechanical forming concepts depending on the chemical composition, strengthening mechanisms, application areas, and geometrical requirements. The formability of thin-walled aluminum sheet depends on its ability to

accommodate the strains experienced during the forming process. This ability depends in turn, on the one hand, on the intrinsic physical properties of the material, such as the strengthening coming from microstructure and chemical composition and, on the other hand, on the external parameters of the forming process.^[48,49] Hence, it is obvious that strain hardening and strain rate hardening, in particular, play an important role in influencing the forming behavior during plastic deformation. These phenomena, and thus the forming behavior, depend on the composition and microstructure, including the grain and precipitate geometry, of the alloys.^[50] Important extrinsic parameters influencing forming behavior include tribological properties, forming temperature, gradients of temperature and strain, as well as blank holding force. Incorrect choice of such parameters can lead to crack initiation and precipitous failure.^[51–54] Given the complex interactions between the external physical variables and the microstructure, control of forming performance using an appropriate choice of thermomechanical parameters is important in many industrial applications. In this section, however, the focus will be on W-temper (WT) forming at room temperature, warm forming (WF), and superplastic forming (SPF).

3.1. Cold Forming of Aluminum

In pure aluminum or aluminum alloys with low strength and high ductility, such as Al–Mg alloys, cold forming enables high surface quality and dimensional accuracy to be attained.

However, the cold forming of heat-treatable, high-strength aluminum alloys in the naturally aged (T4) or precipitation-hardened (T6) state (Figure 6a) is usually limited by poor formability.^[55] The high internal residual stresses in these alloys give rise to a large elastic recovery, known as springback, and a resulting deviation from the desired shape after the workpiece is released from the die. The resulting low-dimensional accuracy is the main reason why the application of high-strength aluminum alloys has been limited in the automotive industry.^[56]

To overcome these drawbacks, the cold-forming step in heat-treatable aluminum alloys can be carried out before aging (Figure 6b).^[57] For this, the sheet material is first solutionized, that is, heat treated at a sufficiently high temperature to put the alloying elements into solution and then quenched to create a supersaturated condition. Since the hardening mechanisms giving rise to a limited formability are initiated only during the subsequent aging process, the deformation of the material takes place in a state of elevated formability. This forming process is referred to as WT forming.^[57] Even in this case, the YS is still high due to the SSS resulting from the alloying elements in solution, so higher forming forces are required than those used for WF, and thermal distortion may appear after subsequent water quenching due to the resulting residual stresses. In addition to WT forming, other techniques used for forming aluminum alloys at room temperature, or even at very low forming temperatures of around $-180\text{ }^{\circ}\text{C}$, include the following: 1) sheet hydroforming; 2) cold stamping using rigid dies; 3) incremental sheet forming; and 4) cryogenic forming.

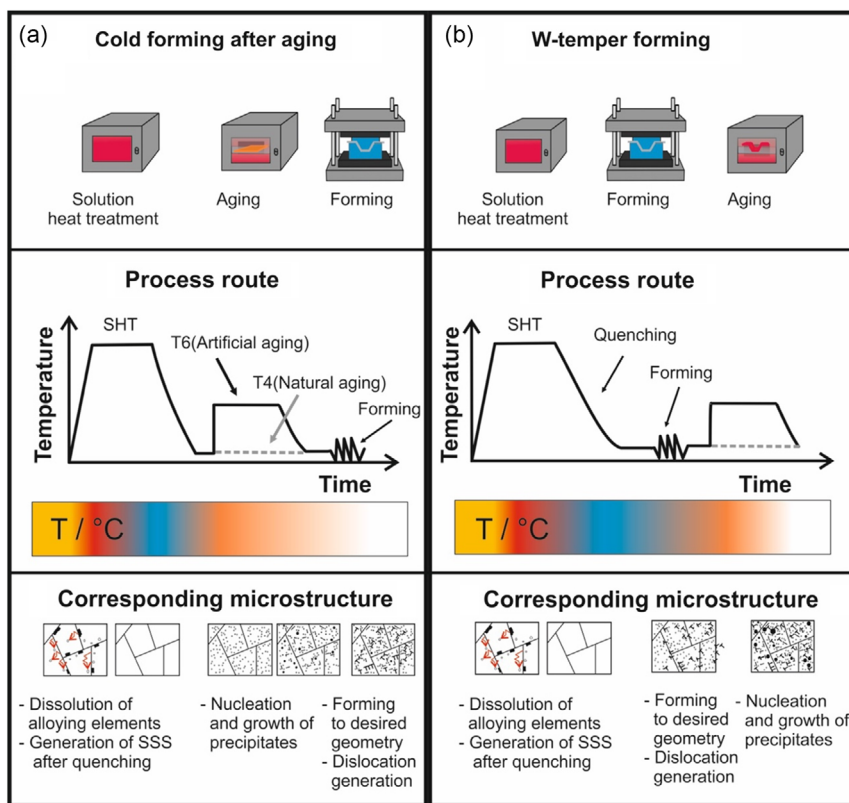


Figure 6. Schematic illustration of the cold forming process in aluminum alloys (a) after and (b) before an aging process.

In the present work, however, only WT forming, which allows the fabrication of complex aluminum parts for mass production in the automotive industry, is discussed in detail. Readers are invited to refer to the following studies for in-depth insights into the other cold forming processes itemized above.^[58–67]

Several experimental and theoretical studies have been carried out to assess the potential of WT forming for the production of industrial parts from precipitation-hardenable aluminum alloys. In another study,^[57] for example, WT forming was compared to cold forming in the T6 condition in the precipitation-hardenable aluminum alloy AA7075 by forming an automotive B-pillar using an industrial tool. While WT forming allowed a crack-free B-pillar to be produced, a completely broken B-pillar was obtained in the T6 cold forming case, due to the appearance of hardening and thinning effects and low formability at room temperature. The Nakajima test, coupled with the digital image correlation technique, is used to evaluate forming behavior and to give insight into deformation and failure mechanisms occurring during forming. This test uses specimens cut from an originally circular test piece into different geometries to give a range of strain states^[68,69] (Figure 7a). The forming limit curves (FLC) obtained by conducting Nakajima tests along different strain paths show that the formability of the precipitation-hardenable aluminum alloy AA7075 using WT forming is significantly higher than that using T6 cold forming (Figure 7b).^[68,70] It can be seen that cracks occur near the center region of the test specimen in all geometries due to the use of lubricant between the die and the specimen.

These results were used in a finite-element (FE) analysis model to predict the thickness distribution during WT forming of a complex-shaped floor tunnel; the results were compared with those obtained using T6 cold forming (Figure 8).^[68] Figure 8a

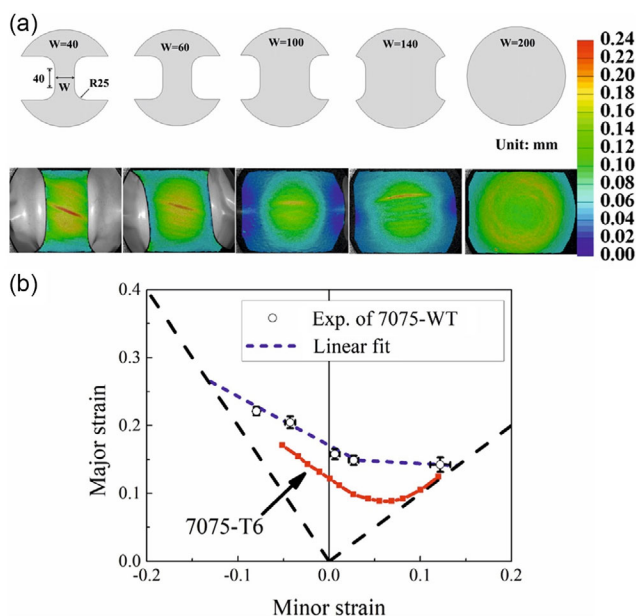


Figure 7. a) Nakajima tests on specimens of different geometries with strain measurement using digital image correlation (AA7075, WT) and b) FLC curves obtained for AA7075 in WT forming and T6 cold forming. Reproduced with permission.^[68] Copyright 2019, Springer Nature.

clearly shows that the model predicts the presence of damage after T6 cold forming, while the experimental results after WT forming (Figure 8b) indicate a damage-free part. Three different yield functions, namely, the von Mises, Hill 1948, and Yld2000-2d functions, were used to predict the thickness distribution. A comparison with experimental results obtained using the ARAMIS 3D digital image correlation system (Figure 8c–f) showed that the nonquadratic Yld2000-2d yield function gave the best agreement with experiment for the thickness distribution, whereas for material wrinkling after forming, all the yield functions gave numerical results of the same order of magnitude.^[68]

It can be concluded from the studies presented above that WT forming is a viable alternative to T6 forming. However, this forming process also has drawbacks. In particular, plastic deformation of the supersaturated solid-solution state at room temperature gives rise to surface phenomena known as shear bands, which propagate on the specimen surface during plastic deformation in the form of localized strain.^[71,72] These occurrences, also known as the Portevin–Le Chatelier (PLC) effect, reduce the surface quality and lead to roughness on the surfaces of the final products.^[73–78] The nucleation and propagation of the bands is followed by a plastic instability, which can be seen in the stress–strain curves as serrated flow and a nonuniform stress profile.^[78,79] This behavior is associated with the interaction of dislocations with solute atoms during plastic deformation.^[75,80] Shear banding can be eliminated by increasing the deformation speed and strain rate during plastic deformation; however, this results in a reduction in the total strain to failure and in pronounced strain hardening that causes complex thinning effects.

Microstructural processes which can affect the forming properties and plastic deformation of precipitation-hardenable aluminum alloys include natural aging, whereby the material strength of the initially as-quenched condition increases over the space of a few hours at room temperature.^[8,81,82] The as-quenched material is supersaturated in precipitate-forming alloying elements such as Mg and Si. These together form coclusters which transform to structures known as GP zones or GP(I) precipitates over periods of only a few minutes after quenching to room temperature.^[83] These small precipitates contribute to the material strength through their interactions with moving dislocations during plastic deformation. The investigations of Banhart et al. have provided detailed insights enabling the understanding of natural aging phenomena in Al–Mg–Si alloys.^[83] To find a suitable process window for heat treatment after quenching, the WT formability of an anticollision door beam was investigated immediately after quenching and after quenching followed by natural aging for periods ranging from 2 to 4 h^[84] (Figure 9a–g). Visible cracks appeared after WT forming with a natural aging time of 4 h (Figure 9g). This was attributed to the increase in strength associated with the formation and growth of GP zones at room temperature.

As discussed above, WT forming enables the production and forming of complex-shaped components in the automotive industry. In addition to the formability of the material, the final mechanical properties of the formed components are also of great importance, as these are used in crash-relevant zones. By adjusting the thermomechanical processing parameters, it is possible to influence the microstructural processes in such

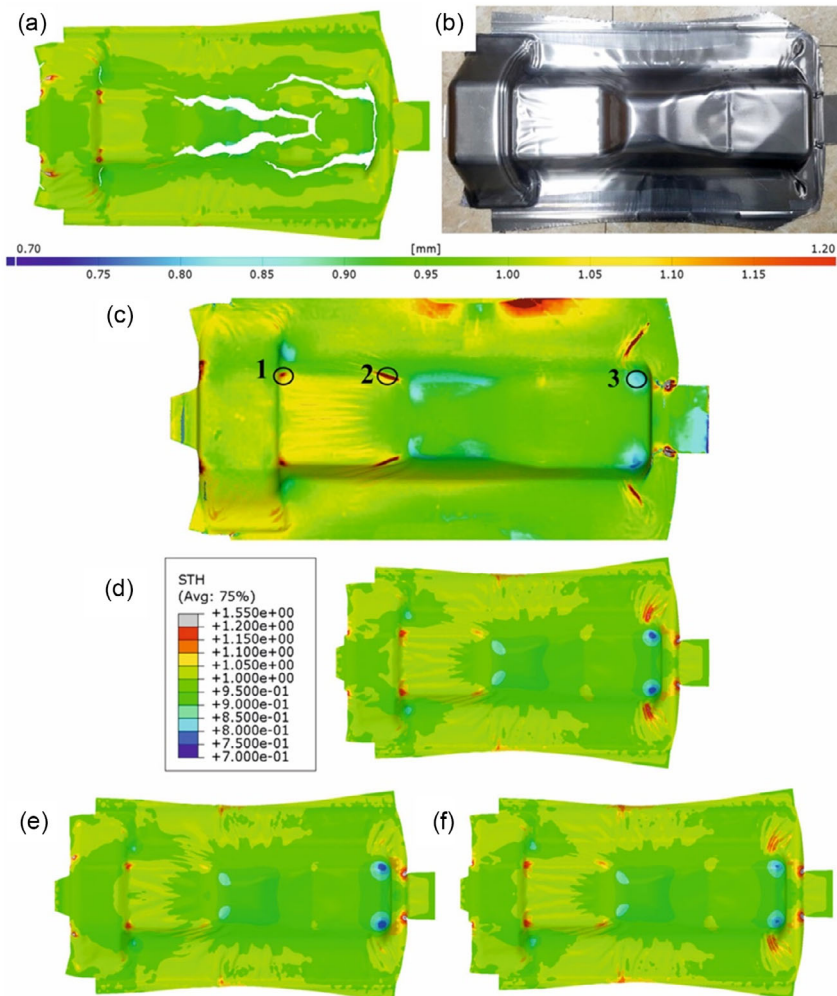


Figure 8. Simulations of forming of parts. a) Predicted T6 cold forming and b) WT forming of a floor tunnel part; c) corresponding thickness distribution obtained experimentally using ARAMIS 3D digital image correlation; corresponding thickness distribution predicted using (d) von Mises, e) Hill 1948, and f) Yld2000-2 d models. Reproduced with permission.^[68] Copyright 2019, Springer Nature.

a way that material strengths comparable to those in the T6 state can be achieved.

In recent work, artificial aging was carried out on the precipitation-hardenable aluminum alloy AA7075 to compare the final mechanical properties after WT forming with those obtained in the T6 state.^[84] In this context, PA (peak aging) refers to an artificial aging treatment carried out at 120 °C for 24 h, which is similar to the conventional artificial aging treatment used to give the T6 state. Paint baking (PB) corresponds to artificial aging at 180 °C for 20 min and shortened artificial aging (SAA) to artificial aging at 120 °C for 20 h. PA alone gives a UTS of 578 MPa. Combining the treatments gives a UTS of 542 MPa for PA&PB (peak aging followed by PB) and 542 MPa for SAA and PB (SAA followed by PB) (Figure 10a,b). Three-point bending results show identical force–displacement curves for PA&PB and SAA&PB; both of these are slightly lower than the force–displacement curve for PA (Figure 10c,d). These results can be explained in terms of the precipitates formed at the chosen artificial aging temperatures. In PB, for example,

the main precipitates found comprise a high volume fraction of the η' -phase^[85] and a small volume fraction of GP(II)^[38] zones, conferring good mechanical properties. For PA&PB, the coarsening of the η' -phase precipitates, which results from the thermal energy input during PB aging, leads to a slight decrease in UTS and bending force compared to PA. However, overall, it can be seen that the selected combinations of aging parameters result in comparable mechanical properties to those in the T6 state.

3.2. Warm and Hot Forming of Aluminum Alloys

At elevated temperatures, it is the interplay of strengthening and softening phenomena which governs the deformation behavior of aluminum alloys. The thermal energy supplied to the material raises the diffusion rate and eases the movement of dislocations by 1) lowering the energy required to overcome microstructural barriers and 2) enabling the activation of further mechanisms by

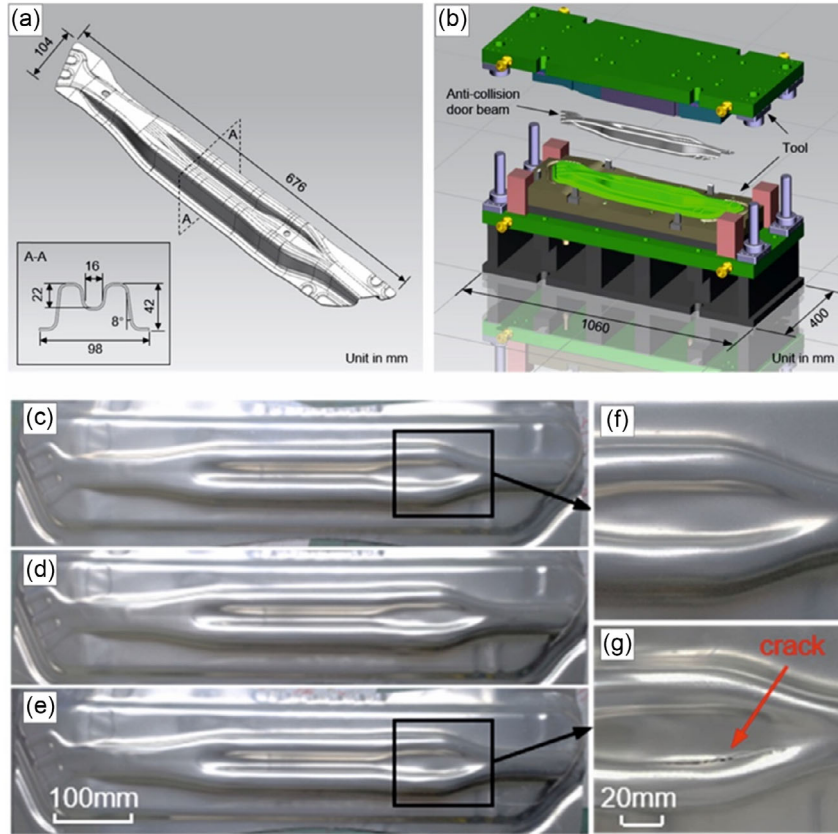


Figure 9. a) Anticollision door beam design, (b) forming tools used, appearance of formed parts after c,d) 0 h, e) 2 h, and f,g) 4 h of natural aging, showing appearance of cracking. Reproduced with permission.^[84] Copyright 2022, Elsevier.

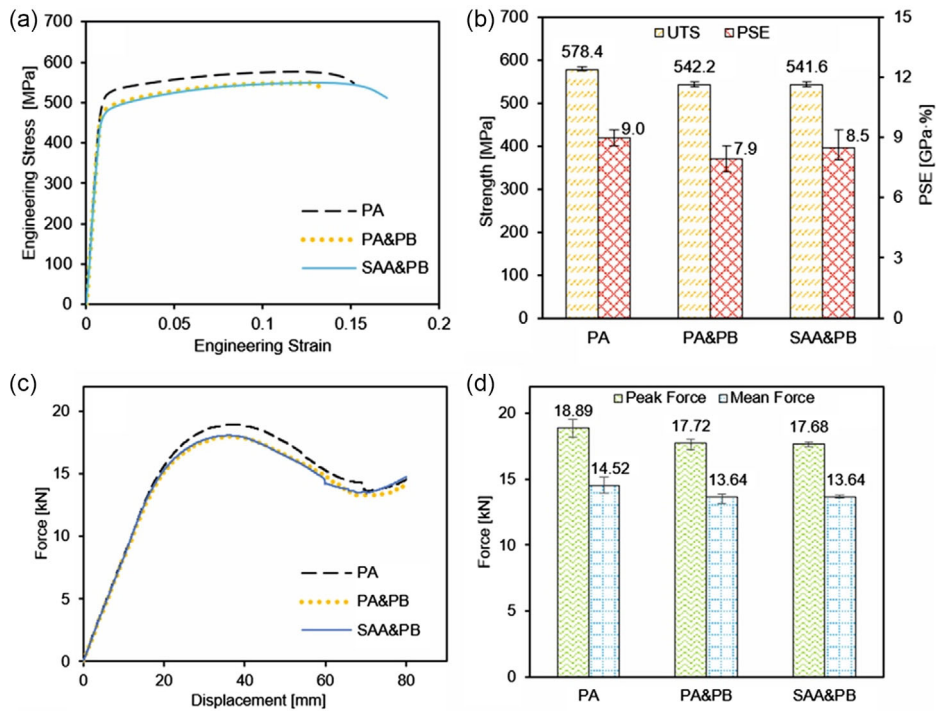


Figure 10. a–b) Tensile properties, c) force–displacement curves, and d) maximum and mean bending forces after WT forming and different aging treatments. Reproduced with permission.^[84] Copyright 2022, Elsevier.

which dislocations may bypass obstacles, such as local or general climb.^[18,33] Thermally activated mechanisms, such as recovery, recrystallization, and precipitate coarsening, lead to a permanent rearrangement of existing defects in the crystal structure, and a reduction in their density, accompanied by a reduction in the effectiveness of work hardening and in the total strength. Also, a greater degree of interaction between the solute atoms, dislocations, and vacancies in aluminum alloys can be assumed.^[86]

Hot forming of aluminum alloys is the controlled deformation of these alloys at temperatures above their recrystallization temperatures. The extensive regeneration of the grain structure, which is accompanied by a reduction in the dislocation density, increases the possible elongation to failure and permits an enhancement in formability. WF, that is, forming at temperatures lower than the recrystallization temperature, prevents dynamic recrystallization, but the higher dislocation mobility still affects the flow stress and elongation to failure, albeit to a smaller extent than in the case of hot forming. Both WF and hot forming are used for heat-treatable and nonheat-treatable aluminum alloys. However, using hot forming for heat-treatable wrought aluminum alloys in their peak-hardened state degrades their mechanical properties by causing growth and coarsening of precipitates beyond their optimum size for strengthening, necessitating further subsequent heat treatments to restore the microstructure and give the desired properties.^[87,88] In addition to dislocation movement, GB sliding may occur in WF and particularly in hot forming;^[89–91] this becomes an increasingly important deformation mechanism in nanocrystalline or ultrafine-grained structures and is used, for example, in quick plastic or superplastic forming.^[92–94]

Since conventional aluminum sheet forming strategies face low formability as a limiting factor when the material strength is high, new strategies have emerged to satisfy the demand for improved properties.^[95–99] These strategies were derived from the original cold forming technology by exploitation of the special strengthening behavior of heat-treatable wrought aluminum alloys and have evolved toward new approaches in warm and hot sheet metal forming. The following section outlines this evolution but concentrates on currently applied thermomechanical approaches.

3.3. Hot Forming and Its Relationship to Microstructural Evolution

Since the beneficial effects of high forming temperatures on formability, in terms of reduced YS and ultimate tensile strength as well as increased elongation, are obvious, hot forming has been investigated in high-strength aluminum alloys as an alternative approach without the drawbacks of cold forming.^[53,100,101] Experimental investigations carried out on a variety of alloys including AA2024,^[102] AA6082,^[103] and AA2060 reveal an increase in strain to failure at high forming temperature with respect to that at room temperature. Higher degrees of deformation enabled more complex-shaped structural components to be formed within one or only a few deformation steps.^[104]

For forming in the lower temperature range of 25–200 °C, the higher end of which is referred to as WF, it has been shown by experimental and numerical investigation of AA5754-O^[105] that the distribution of the tangential stress in the wall of a deformed geometry is the main parameter controlling the springback mechanism. Further numerical and experimental studies have indicated that forming in the range 200–300 °C gives a significant enhancement in formability and drawability of aluminum alloys.^[106–108] Similar findings have been established in investigations on AA7075-T6 and AA6082-T6 formed at different temperatures ranging from RT to 250 °C (**Figure 11**).^[101,109,110] These studies focused on the definition of a temperature range for WF of aluminum alloy sheet based on obtaining an optimal combination of strain hardening behavior and ductility. For this, true stress–strain curves were obtained and Erichsen tests were performed for AA7075-T6 (**Figure 11**).^[110] The true stress–strain curves are divided into four sections to describe the formability mechanisms at the corresponding temperature: 1) elastic section, 2) uniform deformation section, 3) diffuse necking, and 4) localized necking, as shown in **Figure 11a**. A closer look at this classification reveals that the extent of the region of uniform strain (2) initially increases as the temperature increases up to 150 °C and then decreases with increasing temperature to 250 °C. The underlying reasons for this are still being debated by a great number of authors in ongoing studies.^[100,107,111,112] However, in all investigations, a dramatic decrease in UTS and an increase

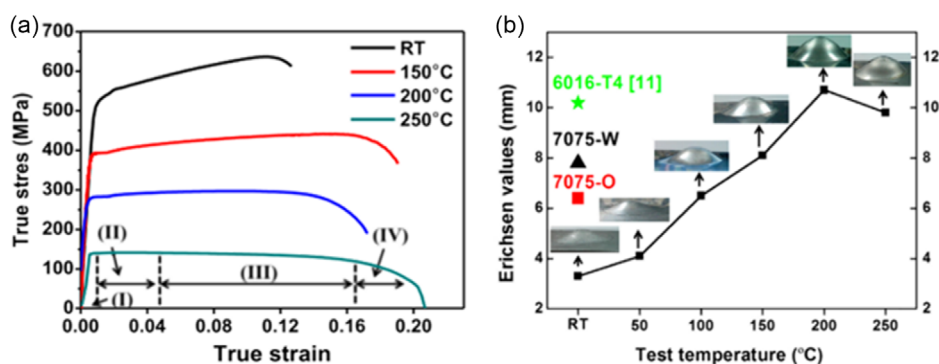


Figure 11. a) True stress–strain behavior of precipitation-hardenable aluminum alloy AA7075-T6 and b) Erichsen test results at different forming temperatures (main curve) as well as results for AA7075-W, AA7075-O, and precipitation-hardenable aluminum alloy AA6016-T4 (labeled points). Adapted with permission.^[110] Copyright 2016, Elsevier.

in elongation to failure is reported with increasing forming temperature in the range from RT to 250 °C.

The influence of forming temperature on strain rate sensitivity and Young's modulus is investigated in another study^[113] for the precipitation-hardenable aluminum alloy AA6111 using the orthogonal anisotropic material model developed by Hill et al.^[114] It is found that a temperature increase from 250 to 500 °C gave a barely significant decrease in elastic modulus of $E = 60$ GPa to $E = 55$ GPa in the blank material investigated. However, with increasing temperature, a significant increase in strain rate sensitivity was observed, leading to a higher YS at an increasing deformation rate.

In order to analyze the underlying microstructural effects, detailed TEM investigations on the warm-formed precipitation-hardenable aluminum alloy AA7075-T6 have been conducted (Figure 12). For 7075-T6, homogeneous matrix precipitates (MPts) with an average size of ~ 5 nm and GB precipitates (GBPs) were observed, responsible for the high strength and low formability of AA7075-T6 at RT. At the elevated temperatures of 200 and 250 °C, an increase in the mean size of MPts and GBPs and in the width of the precipitate-free zone (PFZ) around GBs was observed. The microstructural investigations were expanded in the same study to high-resolution TEM and selected-area diffraction pattern (SADP) analysis (Figure 12). In these micrographs, small-platelet precipitates perpendicular to the $\{111\}_{Al}$ planes are found. Based on the forming temperatures, these precipitates were classified as GP zones (transforming to η'), η' , and stable hexagonal η -phases.^[38,85,110]

3.4. Hot Deformation and Hardening Behavior of Aluminum Alloys at High Temperatures

As outlined above, microstructural processes such as dynamic recovery, dynamic recrystallization, and PH affect the flow behavior as well as the strain-hardening behavior of aluminum alloys during WF. At forming temperatures above 300 or 350 °C, these

thermally activated processes and solid-state reactions are accelerated due to the high thermal energy provided and the consequent increased diffusion rates, leading to significant changes in grain structure, precipitate species present, and precipitate morphology as well as in the flow stress.^[115–117] In addition to this, depending on the heat treatment conditions applied to precipitation-hardenable aluminum alloys, the influence of dynamic precipitation on the flow stress may need to be taken into consideration.^[118,119]

The hot deformation behavior that takes place during hot or WF processes, and the associated thermophysical mechanisms, as well as the microstructural processes involved, are found to be very complex. They can be influenced by the strain rate $\dot{\epsilon}$, forming temperature T , and the degree of plastic deformation experienced by the material during thermomechanical processing. In another study,^[116] therefore, the effect of deformation temperatures ranging from 200 to 400 °C and strain rates of $\dot{\epsilon} = 0.01$ s⁻¹, $\dot{\epsilon} = 0.01$ s⁻¹ and $\dot{\epsilon} = 0.1$ s⁻¹ on the hot deformation behavior of precipitation-hardenable aluminum alloy AA7075 were investigated (Figure 13).^[120]

To characterize the hot formability for hot stamping of the material in different microstructural states, the hot deformation behaviors of an AA7075 alloy supplied in the in peak-aged T6 condition (Figure 13a), and in the as-quenched condition (after solution heat treatment) (Figure 13b), were compared. In both conditions, a decrease in flow stress with increasing deformation temperature and decreasing strain rate was observed; this is typical for aluminum alloys. These phenomena, also seen at the same temperature and strain rate range elsewhere,^[121–123] are associated with increased lattice vibrations and dislocation mobility arising from thermal activation as well as to the time required for the activation of the softening mechanisms. At higher deformation temperatures, the increased thermal energy significantly reduces the mechanical energy required for dislocations to move through the material during plastic deformation and leads to increased activation of cross-slip of screw dislocations. The effect

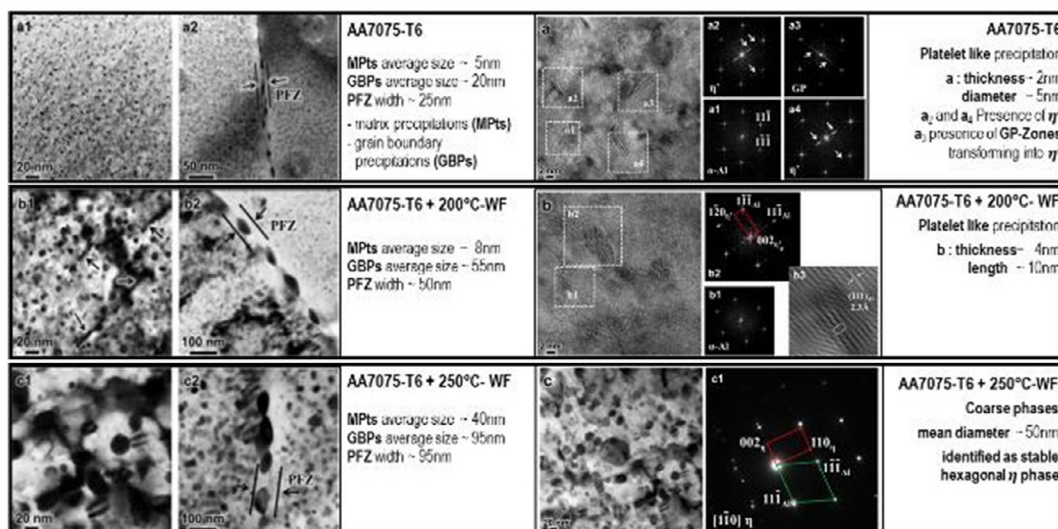


Figure 12. TEM micrographs from AA7075-T6 deformed at different temperatures.^[110] An increase in the size of matrix precipitates (MPts) and GBPs was observed with increasing WF temperature. Adapted with permission.^[110] Copyright 2016, Elsevier.

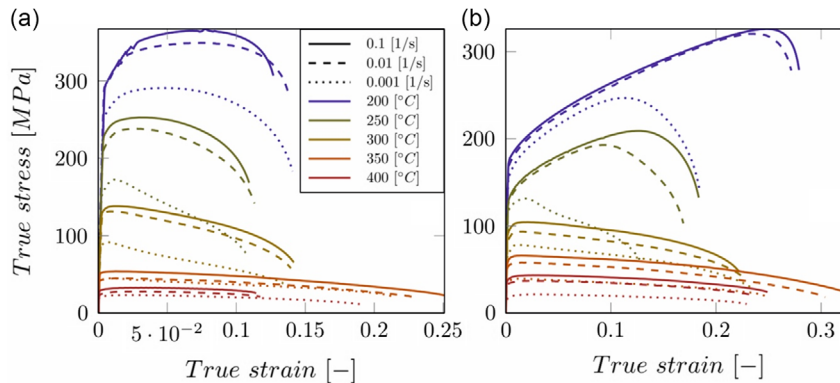


Figure 13. Hot deformation tensile behavior of precipitation-hardenable aluminum alloy AA7075 in a) T6 condition (solution heat treated, quenched, and artificially peak aged) and b) as-quenched condition (solution heat treated and quenched) at different forming temperatures ranging from 200 to 400 °C and strain rates from $\dot{\epsilon} = 0.01\text{s}^{-1}$ to $\dot{\epsilon} = 0.1\text{s}^{-1}$. Reproduced with permission.^[116,120] Copyright 2022, MDPI.

of the strain rate on the flow behavior can be rationalized by considering the time required for the activation of thermally activated phenomena and the effect of thermal energy on the probability of slip processes per unit time. Decreasing the strain rate while maintaining the same deformation temperature gives more time for thermally activated softening processes such as recrystallization and dynamic recovery, increasing, leading to lower flow stress, as can be seen in (Figure 13a,b), for both the peak-aged and as-quenched conditions.

Dynamic recrystallization in aluminum alloys is observed in the vicinity of GBs as well as within the grain interiors. The nucleation of recrystallized grains is believed to occur through a GB bulging mechanism, which is characteristic of discontinuous dynamic recrystallization.^[124] The high-stacking-fault energy of aluminum alloys favors a high rate of dynamic recovery through dislocation climb and cross-slip. As a result of this and of the low mobility of GBs, precipitation-hardenable aluminum alloys are more susceptible to continuous dynamic recrystallization than to discontinuous recrystallization.^[125] The presence of different types of precipitates, which may nucleate and grow during hot deformation, hinders the migration of GBs and explains the absence of discontinuous dynamic recrystallization.^[125] Experimental studies on single-crystal aluminum during compression tests show that the formation of fine and homogeneously distributed precipitates prior to hot deformation leads to a nearly complete suppression of recrystallization in the precipitation-hardenable 7xxx series alloys.^[126] In the previously mentioned studies, however, the microstructure of the precipitation-hardenable aluminum alloy A7075 after deformation at a temperature of 400 °C shows a high fraction of dynamically recrystallized grains for both the T6 peak-aged and the as-quenched conditions (Figure 14).

At higher forming temperatures ranging from 450 to 520 °C, different types of dynamic recrystallization phenomena, including continuous, discontinuous, and geometrical dynamic recrystallization,^[127,128] are believed to occur in the precipitation-hardenable aluminum alloy AA7075.^[129] However, continuous dynamic recrystallization is reported to be the main softening mechanism, while the occurrence of geometrical dynamic

recrystallization is reported only at deformation temperatures below 520 °C.^[129]

Returning to the hot deformation behavior of precipitation-hardenable aluminum alloy AA7075 in different microstructural states, in Figure 13b, the hot deformation behavior at 200 °C and a strain rate of $\dot{\epsilon} = 0.01\text{s}^{-1}$ show a significant increase in the flow stress during plastic deformation. This behavior is linked to the formation of small precipitates, which is driven by a sufficiently high thermal energy and defect density within the crystal structure, that is, stored strain energy. At the same time, a high degree of elongation after failure is achieved, comparable to values attained at the much higher temperature of 420 °C.^[130,131] For industrial applications, it is clear from the investigations presented above that the underlying microstructural condition of precipitation-hardenable aluminum alloys significantly affects the flow behavior. At a low forming temperature of 200 °C and low strain rate of $\dot{\epsilon} = 0.001\text{s}^{-1}$, an increased degree of hardening during forming, due to dynamic precipitation, could lead to inhomogeneous forming behavior as well as premature failure. At a higher forming temperature of 420 °C and strain rates of $\dot{\epsilon} = 0.001\text{s}^{-1}$, by contrast, the greater elongation to failure and reduced degree of hardening avoid these problems, allowing the design of more complex structures with higher degrees of deformation.

To take account of microstructural effects in process design, the hot deformation and strain hardening behavior of AA7075 in the as-quenched state were investigated to determine the formability behavior during hot compression at high strain rates up to $\dot{\epsilon} = 10\text{s}^{-1}$.^[119,132,133] In [134] in addition, a thermally stabilized condition is used to compare the hardening effects and precipitation–dislocation interactions during hot compression to those in the as-quenched condition. The thermally stabilized condition, obtained by solution heat treatment, water quenching, and artificial aging for 24 h at the intended deformation temperature, was designed to prevent precipitate nucleation and growth during hot compression. The hardening behavior during hot forming is usually represented in terms of the strain hardening rate, which is obtained from the derivative of fitted true stress–strain curves.^[132,133,135,136] These investigations allow

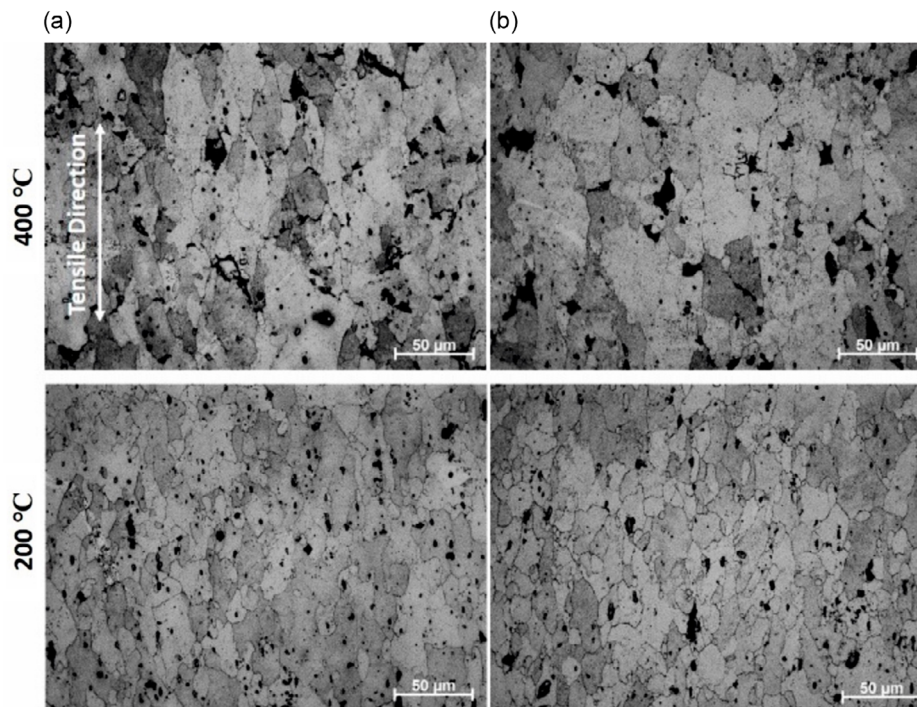


Figure 14. Optical micrographs of a) T6 peak-aged condition and b) as-quenched condition after deformation at 200 and 400 °C. Reproduced with permission.^[116] Copyright 2020, MDPI.

the characterization and determination of the influence of microstructure and precipitation processes during hot deformation on the onset of dynamic recovery and recrystallization. A high dislocation mobility in the initial stages of plastic deformation in the as-quenched condition leads to the occurrence of dynamic recrystallization at lower critical stresses. However, a higher strain hardening rate is found in the stabilized microstructure with increasing plastic deformation.

It can thus be concluded that the formation of nanoscopic precipitates in the thermodynamically unstable supersaturated solution affects not only the recrystallization process but also dislocation–dislocation and dislocation–precipitate interactions in precipitation-hardenable aluminum alloys. In addition, the choice of deformation temperature and strain rate determines the time of onset of deformation-induced hardening and softening mechanisms and leads to correspondingly high or low flow stress values during plastic deformation. From these results, the fundamental impact of the microstructural condition on the flow behavior of precipitation-hardenable aluminum alloys at different deformation temperatures and strain rates can be understood.

3.5. Superplastic and Quick Plastic Forming

Another approach to extend the limits of aluminum alloys is SPF (Figure 15). The main advantage of this technique is its capability to shape complex geometries, thanks to the increase in formability that it confers at elevated temperatures.^[137,138] It is carried out at the solution-heat-treatment temperature using an isothermal forming operation at low strain rates, that is, of the order of

$\dot{\epsilon} = 10^{-3}$ to $\dot{\epsilon} = 10^{-4}$.^[23,139–141] Gas pressure, applied between die and sheet surface, deforms the material, pushing it into a heated die cavity (Figure 15c). In this way, very high elongations to failure of up to 200% are obtained through microstructural mechanisms such as cooperative GB sliding (Figure 15b). With decreasing grain size and strain rate, these phenomena become even more pronounced.

The SPF technique is usually applied in low- and medium-strength aluminum alloys such as the 2xxx, 5xxx, and 6xxx series. Using this technique in the high-strength, heat-treatable aluminum alloys of the 7xxx series require an optimal balance between forming temperature and speed.^[142–144] To overcome the excessive thinning and necking that can occur in traditional single-stage forming in the 7xxx series, as well as to improve the forming behavior, a two-stage SPF process has been developed.^[145] The final mechanical properties are adjusted after SPF through an aging treatment; however, this increases the total duration of the process and increases the risk of thermal distortion. Because of this, and because of the requirement for costly heated forming tools, the low deformation rate, and long cycle times, SPF is limited only to small series or prototype production.

Due to the demand of the automotive industry for high production rates, General Motors developed a technique known as Quick plastic forming, (Figure 15d), which combines SPF and hot deep drawing at higher forming rates (of $\dot{\epsilon} = 10^{-3}$) than SPF.^[146–148] This technology allows the design of complex-shaped components at even lower cost, simpler tools, higher forming rates, and markedly higher production efficiency thanks to short production cycle times.^[147] In this technique, preheated (450 to 510 °C) aluminum blanks are transferred into the

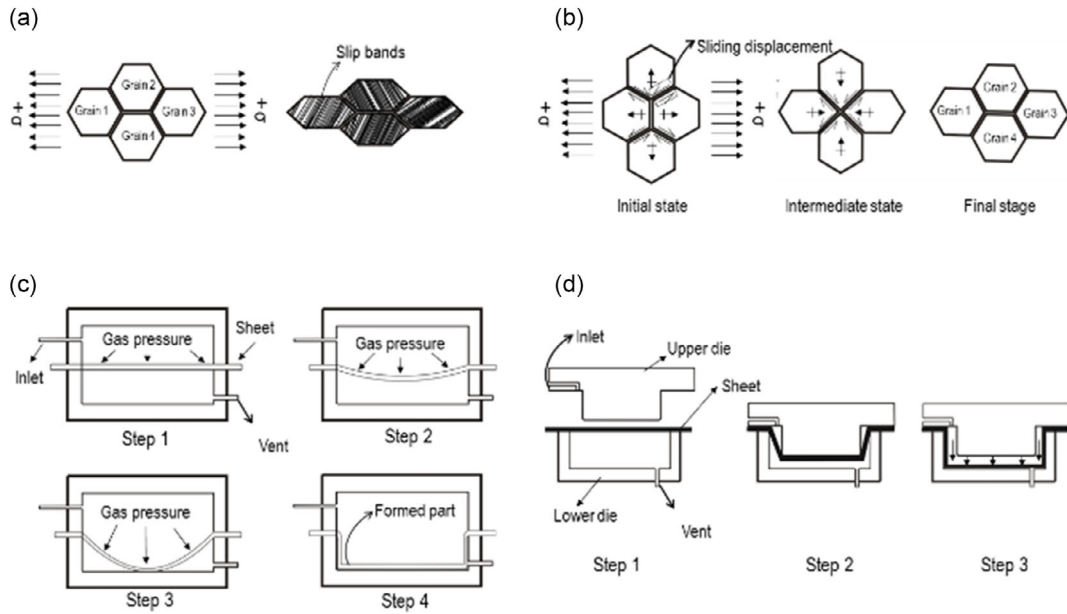


Figure 15. Schematic comparison of microstructural evolution in a) plastic deformation and b) superplastic deformation. Illustration of the process steps of c) SPF and d) quick plastic forming.

hydraulic press and deformed using a heated top die. The final geometry is obtained by applying an additional gas pressure (Figure 15d). After the forming operation, the parts are cooled using purpose-built cooling fixtures.

4. Hot Forming–Quenching of Aluminum Alloys

As the effectiveness of cold forming of heat-treatable wrought aluminum alloys is limited by low formability and the high degree of springback, and conventional hot forming processes affect the microstructural phenomena as described above,

ongoing research has focused on the development of a thermo-mechanical (hot) forming process approach that integrates the process route required to give PH.^[88,149–154] This process, first proposed by Lin et al.^[149] as HFQ, primarily consists of three steps, shown schematically in **Figure 16**. The first step consists of solution annealing (solution heat treatment), whereby the material is heated at a sufficiently high temperature to dissolve the alloying elements and form a single-phase solid solution. In the second step, quenching and hot forming are combined within one step using the forming tools as quenching media. After the blank has been formed into the desired geometry, it is held within the closed tool for sufficient time to ensure that

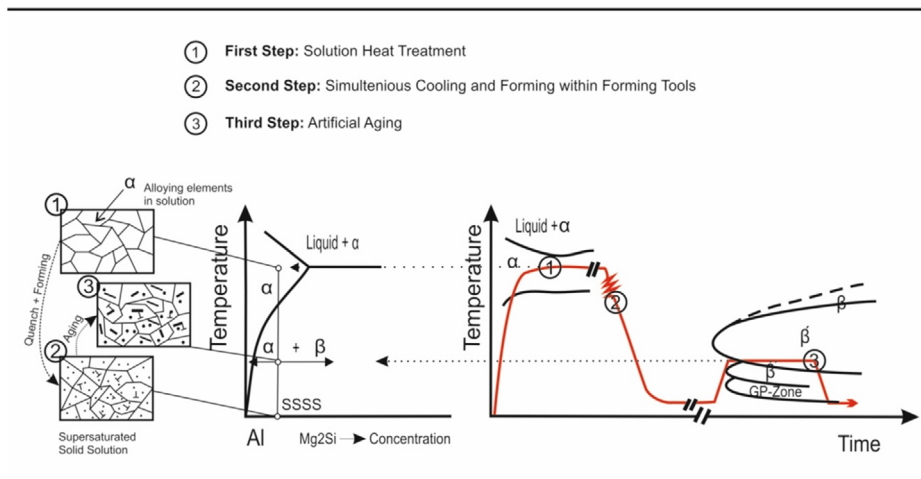


Figure 16. Schematic illustration of the HFQ forming process route.^[14] In the first step, the sheet material is heated to its solution heat treatment temperature and held for sufficient time to homogenize and dissolve the alloying elements into solid solution. The heated sheet is then formed and quenched within the forming tools in a single step to create the SSSS state and reduce the distortion that would otherwise occur due to thermal gradients. Finally, if the material is age hardenable, it is then aged to obtain the desired properties, usually peak strength.

the cooling rate is high enough to obtain the unstable microstructural condition known as a supersaturated solid solution (SSSS). In the third step, only performed in age-hardenable alloys, an age-hardening process is carried out to give optimal mechanical properties. This approach can be applied to all precipitation-hardenable alloys as well as to nonage-hardenable aluminum alloys of the 5xxx-series^[14,99,155–157] and even magnesium alloys.^[156]

Since the first appearance of this technique, many studies have compared its performance to that of conventional processes. In another study,^[158] for example, the formability of Al6061 in artificially aged (T6) and naturally aged (T4) input conditions and the dimensional accuracy of the final products are compared for the HFQ forming process and conventional cold forming. Hardness measurements in this study showed a slight increase after HFQ forming with respect to the T6 condition. Wang et al.^[159] demonstrated, in a detailed study, the positive effects of the HFQ forming process route on springback and geometrical accuracy in AA5754. A remarkable decrease in springback in the final geometry was attained with high blank temperatures, high forming speeds, and smaller die gaps in this material. Further studies have confirmed this behavior for AA7075 and AA6082 alloys (Figure 17).^[87,160]

The potential of the HFQ forming process is not limited to the automotive industry,^[161] but has also found interest in the aerospace industry, where components of particularly complex shape are required. In other studies,^[102,104] the forming temperature that would give optimum forming and mechanical behavior was investigated for wing stiffener components made from

AA2060. For this purpose, a two-step variant of the process was used to form the requisite complex geometry. In the first step, the sheet was heated to a temperature of 470 °C, which is slightly below the solution heat treatment temperature, and formed within the cooled tools to the desired geometry. In the second step, the formed blank was reheated to its solution heat treatment temperature (520 °C, 1 min), to dissolve the alloying elements. The formed part was then quenched to room temperature to achieve the SSSS condition in preparation for the subsequent aging treatment at 180 °C. The final mechanical properties obtained using the two-step process were almost the same as those of the as-received (AA2060-T8) material (Figure 18) and required an even shorter aging time to attain the peak hardness (Figure 18b).

Following the development of this two-step forming route for complex-shaped components, finite-element (FE) modeling was conducted to determine the thinning behavior of the same geometry during the forming process.^[156] Both numerical and experimental results for AA5754 showed a decrease in the extent of local thinning with increasing strain rate and decreasing forming temperature (Figure 19). The combined effect of a higher degree of higher strain hardening and lower heat transfer between the hot blank and the cold tools led to a higher material draw-in and a lower degree of local thinning.^[156] Further numerical and experimental investigations were conducted to investigate the thickness distribution in complex-shaped components of AA6082 after both the new hot forming process and cold forming.^[162] The FE model developed showed good agreement with the experimental results obtained after hot forming

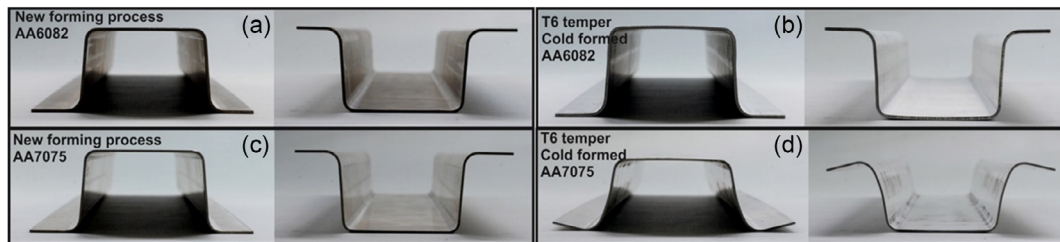


Figure 17. Illustration and comparison of the formed parts after using the HFQ process in a) AA6082 and c) AA7075 versus the b) conventional forming process AA6082 and d) AA 7075 at room temperature. Reproduced with permission.^[87] Copyright 2017, Wissenschaftliche Scripten. The hot-formed geometries produced using the novel forming process indicate nearly no springback, in contrast to the cold-formed parts.

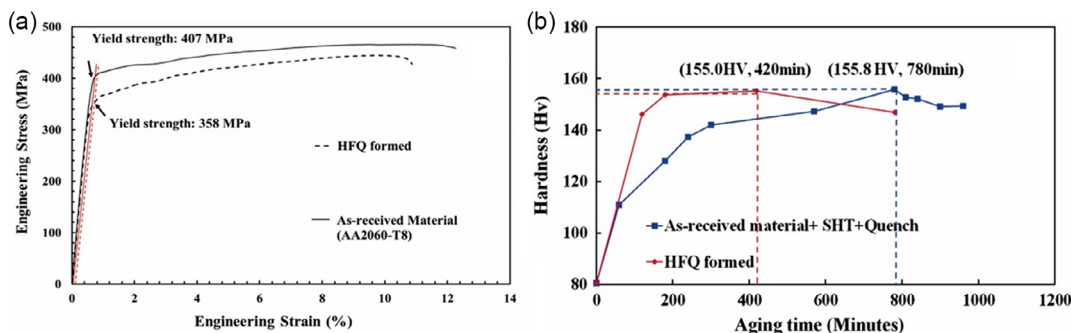


Figure 18. Comparison of the final mechanical properties of AA2060 produced using the HFQ forming process and those of the as-received material. The a) tensile curves show almost the same behavior in the formed as in the as-received condition. b) Hardness measurements carried out after aging AA2060 at 180 °C for different aging times show a decrease in time needed to attain peak aging condition using the new process. Reproduced with permission.^[104] Copyright 2016, EDP Sciences.

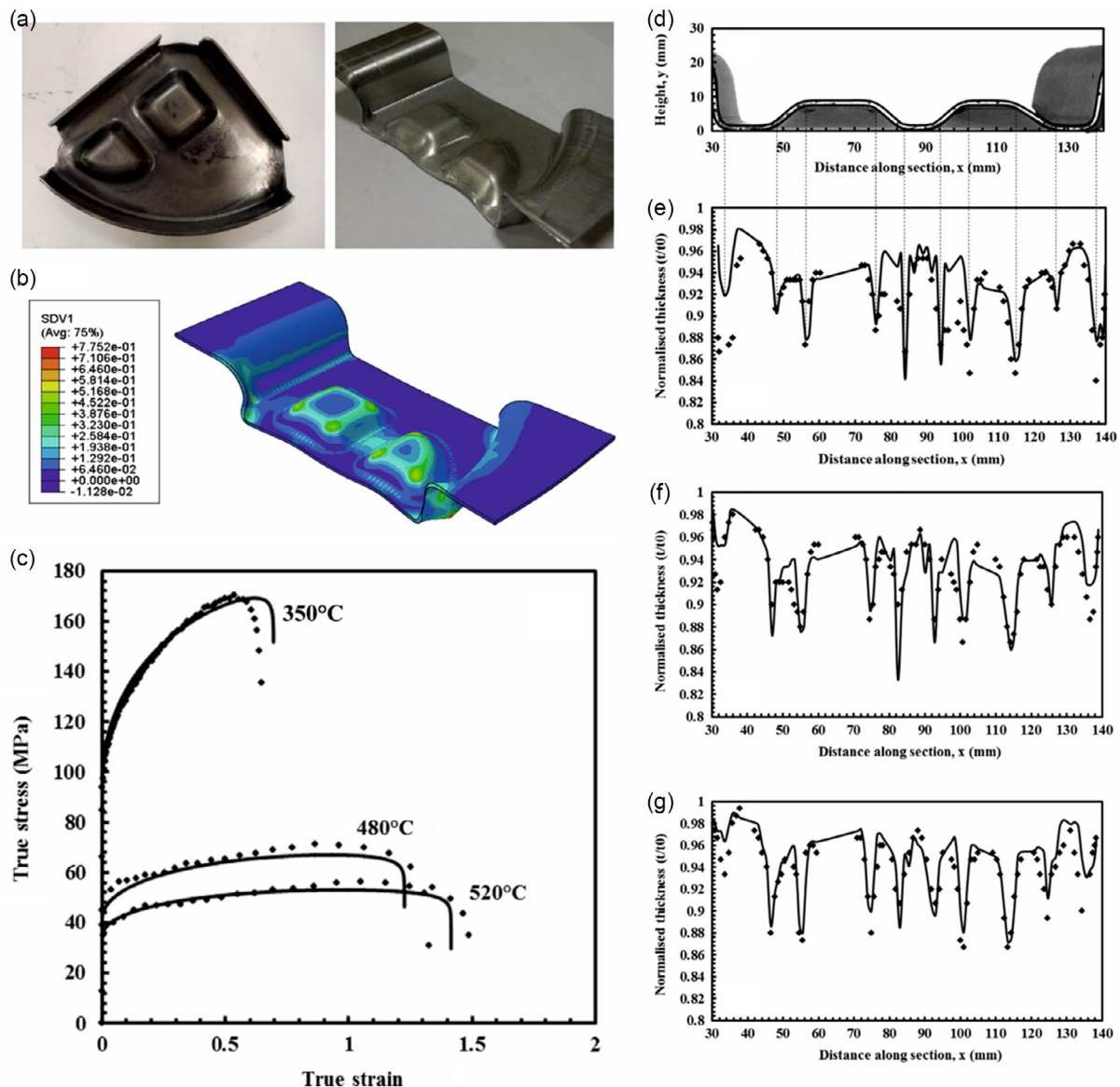


Figure 19. Illustration of successfully formed a,b) complex-shaped component (wing stiffener) produced using the HFQ forming process in two steps. Adapted with permission.^[153] Copyright 2014, Elsevier. Reproduced with permission.^[104] Copyright 2016, EDP Sciences. Comparison of calculated and experimental stress–strain behavior c) of AA5754 at different forming temperatures. Numerically calculated thickness distribution in the complex-shaped geometry investigated along the cross section of the formed component at different forming temperatures: e) 480 °C, f) 350 °C, and g) 200 °C and at a forming speed of 250 mm s⁻¹. Adapted with permission.^[153] Copyright 2014, Elsevier.

(Figure 20). In addition, this study demonstrated the advantages of the new process, in terms of better formability, over the traditional cold forming process for complex-shaped components (Figure 20c,d).

4.1. Process Variants and Influence of Process Parameters

4.1.1. Effect of Heating Rates

The complete dissolution of the alloying elements and the generation of a homogeneous single phase is the key requirement for a successful solution annealing treatment. This can be

achieved by heating the alloy above its solution heat treatment temperature. The higher the supersaturation of the alloy in the quenched state, the higher the potential for PH. From the economic point of view, a high heating rate can save energy and costs by reducing the required heating time and thus the total process time. The effects of different heating rates (0.2, 2, and 20 °C s⁻¹) and soaking times on the tensile performance of AA6082-T6 sheet material were investigated in another study.^[163] It was shown, by measuring the resulting mechanical properties, that the treatment time required to achieve complete dissolution decreased with increasing heating rate. Higher hardness was observed after the entire HFQ process and artificial

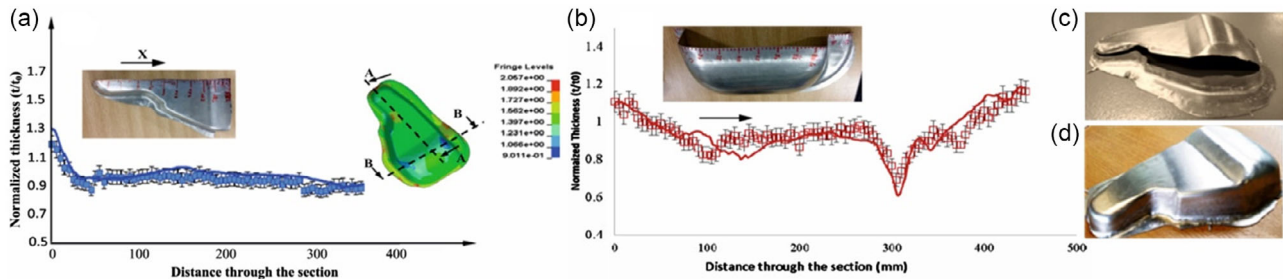


Figure 20. Comparison of experimental and FE simulation results giving local thinning distribution in an AA6082 component after forming using the HFQ process. Reproduced with permission.^[162] Copyright 2015, Mohamed et al., published by EDP Sciences. Illustration of the formed geometry after a) cold forming and after application of the b) HFQ process. Reproduced with permission.^[162] Copyright 2015, EDP Sciences.

aging for a high heating rate ($20\text{ }^{\circ}\text{C s}^{-1}$) at a given soaking time of, for example, 2 min than for a lower heating rate ($0.2\text{ }^{\circ}\text{C s}^{-1}$). The explanation for this observation was that higher heating rates ($20\text{ }^{\circ}\text{C s}^{-1}$) avoided the formation, during heating to the SHT temperature, of β' and β phases from the coarse, hard-to-dissolve β'' phase.

The influence of the heating rate on the microstructural evolution of Al–Cu and Al–Cu–Zr–Ti–V alloys was investigated using scanning electron microscopy (SEM), electron beam microanalysis (ESMA), and TEM by Zhao et al.^[113] The improvement in hardness and, therefore, reduction in the required solutionizing time achieved using high heating rates was found to be related to an increased density of vacancies and other defects such as vacancy clusters, as well as stronger interaction between dislocations and vacancies in the matrix. In addition, higher heating rates affected the nature, nucleation and growth rates, and distribution of precipitates in the alloys investigated.

4.1.2. Effect of Solution Heat Treatment Temperature

The solution heat treatment temperature is another factor affecting the dissolution of precipitates. Temperatures lower than the solvus temperature of the most stable precipitate phase will lead to incomplete dissolution of the precipitates and will limit the degree of age hardening that is subsequently possible. In contrast, excessively high solution heat treatment temperatures may result in incipient eutectic melting, which causes a dramatic

degradation of mechanical properties, in particular a sharp decrease in the elongation to failure, as well as requiring more energy and time than necessary. Therefore, it is crucial to find the optimum solution heat treatment temperature; this depends primarily on the alloy composition as well as on the size and distribution of the second phases present in the microstructure before solutionizing.^[53,164–166]

The effects of solution heat treatment temperatures ranging from 525 to 570 °C in AA6082 O were investigated in another study.^[163] Similarly to the heating rates, higher solution heat treatment temperatures decreased the required soaking time. At a high solution heat treatment temperature of 570 °C, the required soaking time was 1 min, whereas at a lower temperature of 525 °C, a soaking time of 20 min was required to achieve approximately the same mechanical properties after artificial aging (Figure 21). Increasing the solution heat treatment time beyond 20 min had no further significant effect on the mechanical behavior.

The reason for this was that higher solution heat treatment temperatures give a higher diffusivity for all atomic species. In addition, a higher equilibrium concentration of vacancies, which facilitate diffusion, is present in the lattice structure at higher temperatures. As a result, a shorter time is required for full dissolution of precipitates at higher temperatures.

The influence of solution heat treatment temperature on yield and tensile strength and elongation in AA6082 and AA7075 was analyzed in another study.^[167] (Figure 22). It was shown that higher solution heat treatment temperatures gave better mechanical properties than lower temperatures; this effect was

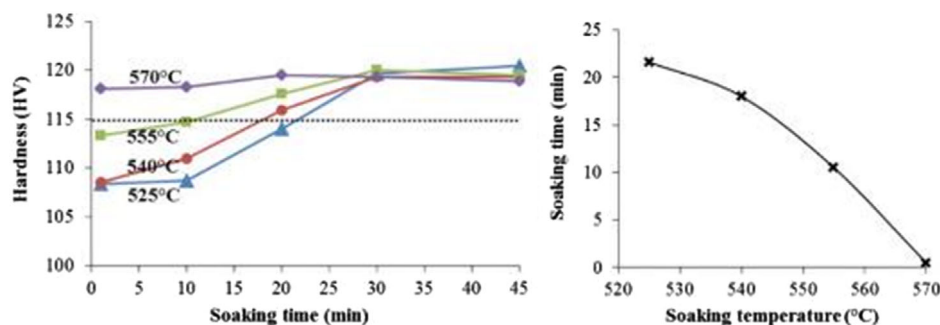


Figure 21. Influence of different solution heat temperatures on a) mechanical properties after artificial aging and b) soaking time of AA6082. Reproduced with permission.^[163] Copyright 2015, EDP Sciences.

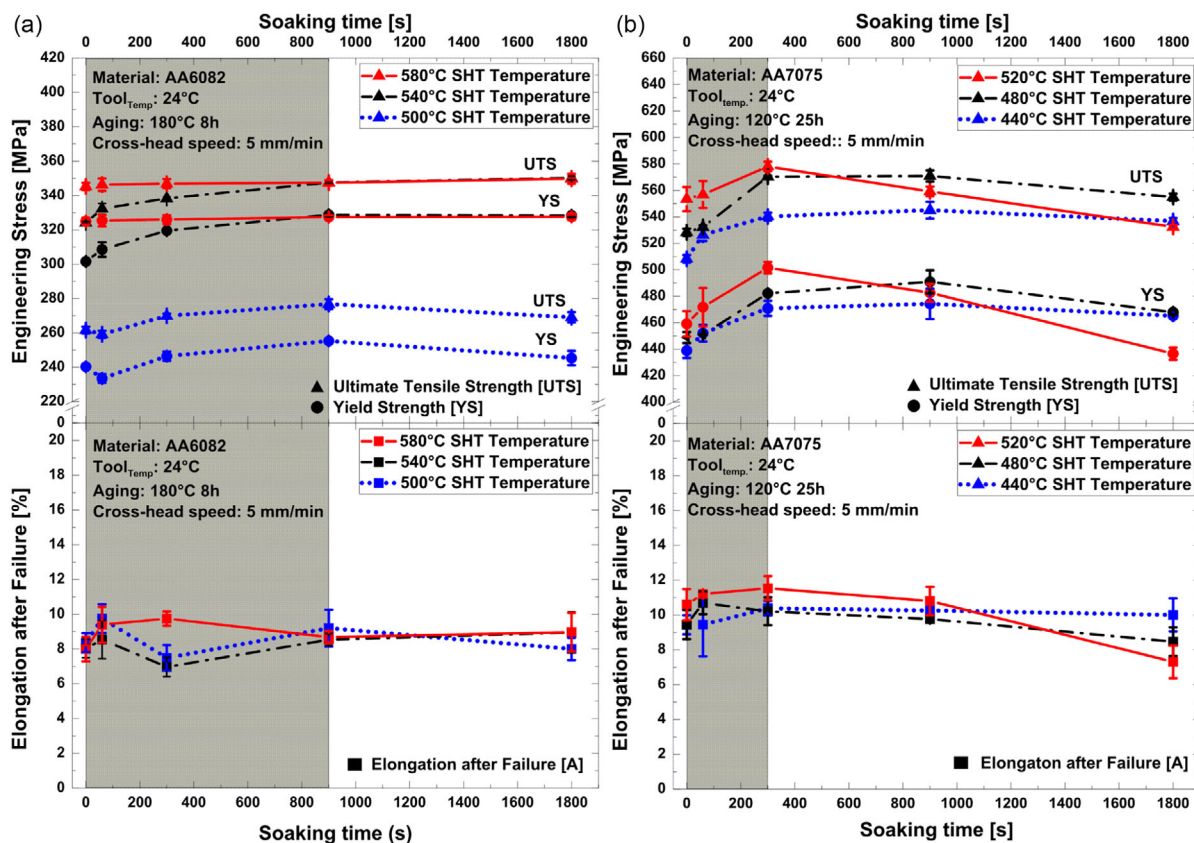


Figure 22. Influence of solution heat treatment temperature on mechanical properties in a) AA6082 and b) AA7075. Reproduced with permission.^[167] Copyright 2019, Elsevier.

pronounced for AA6082 at 500 °C. This confirmed earlier findings, described above, that at lower solution heat treatment temperatures, the precipitates cannot fully dissolve, and hence the material does not attain its full potential for PH after quenching. Increasing the solution heat treatment temperature above the solvus temperature of the most stable precipitates enabled shorter solution heat treatment temperatures times due to the effects explained earlier.^[167]

In order to investigate the influence of solution heat treatment time on the strengthening mechanisms, experimental studies have compared the mechanical behavior of 6A02 aluminum alloy after soaking at different times (520 °C for 5, 25, and 50 min),

cooling at a rate of 50 °C s⁻¹, and aging at 160 °C for 10 h.^[168,169] It was shown that increasing the solution heat treatment time at a given cooling rate led to an increase in hardness and in ultimate tensile strength. The reason for this is that once the alloy reaches the solution heat treatment temperature, the diffusion rate of the alloying elements increases. Longer soaking times mean that enough thermal energy is supplied to give complete dissolution of the second phase. This behavior is shown in another study,^[168] in which SEM observations reveal a higher volume fraction of coarse second-phase precipitates after a solution heat treatment time of 5 min (Figure 23a), than are present at longer solution treatment times in Figure 23b,c. However, it

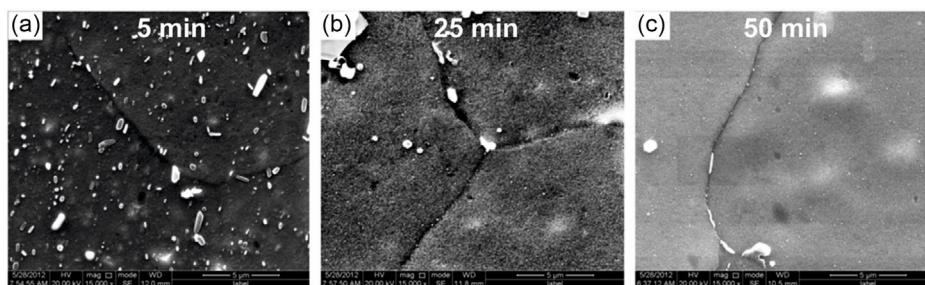


Figure 23. SEM observations of the aged condition of 6A02 aluminum alloy after solution treatment for different times: a) 5 min, b) 25 min, and c) 50 min. Reproduced (Adapted) with permission.^[168] Copyright 2016, Elsevier.

should be noted that the initial microstructure of the as-received material already exhibits coarse second phases. This can be explained by the relatively long treatment time needed to dissolve the precipitates into the solid solution and to complete the solution treatment.

4.1.3. Influence of Cooling Strategy on Mechanical Properties and Microstructure

To obtain the desired final mechanical properties, it is essential to suppress, using sufficiently high cooling rates, the formation of precipitates, especially at GBs, after the complete dissolution of the alloying elements. This preserves the supersaturated state and maintains a high concentration of vacancies. This supersaturated condition promotes the finely dispersed, homogenous nucleation of precipitates during the subsequent aging process. The required cooling rates are usually provided using cooled forming tools during the combined forming and quenching step. In other studies,^[15,85] for example, the effect of different cooling strategies (water quenching, quenching between flat cold steel dies, and quenching in air) on the final mechanical and microstructural properties of AA6082 is compared after aging at 190 °C for 9 h. The mechanical properties obtained (YS = 200 MPa, UTS = 290 MPa, and strain to failure $\epsilon_f = 0.18\%$) after using the

cold die quenching technique are only slightly lower than those obtained using the water quenching method (YS = 230 MPa, TS = 305 MPa, and strain to failure $\epsilon_f = 0.17\%$). A further study^[150] focused on the investigation of the effects of different die clearances (from 0 to 2.0 mm) and loads (from 2 to 10 tons) on the quenching rate in AA6082. The cooling rate increased with increasing applied load and decreasing die clearance, but only to a certain limit. Tensile tests revealed that the tensile strength of the material also increased with increasing cooling rate.

Figure 24a shows an example using different die temperatures.^[170] In order to maintain the forming temperature sufficiently high to ensure formability of the blank, the heat loss should be reduced to a minimum. For this reason, research has focused on the influence of tool temperatures on the final properties of different aluminum alloys in the 2xxx and 6xxx series as well as Al-Cu-Mg alloys.^[168,170–172] The use of heated tools (Figure 24b) prevented the rapid cooling of the sheet material during the first contact and thereby improved the formability. The studies in other studies^[168,170–172] investigated the effect of die temperature (from 50 to 350 °C) on cooling rate and maintenance of formability by comparing the mechanical and microstructural behavior. The temperature difference between the blank and the heated dies is found to strongly influence the cooling rate (Figure 24e). A higher cooling rate and an increasing

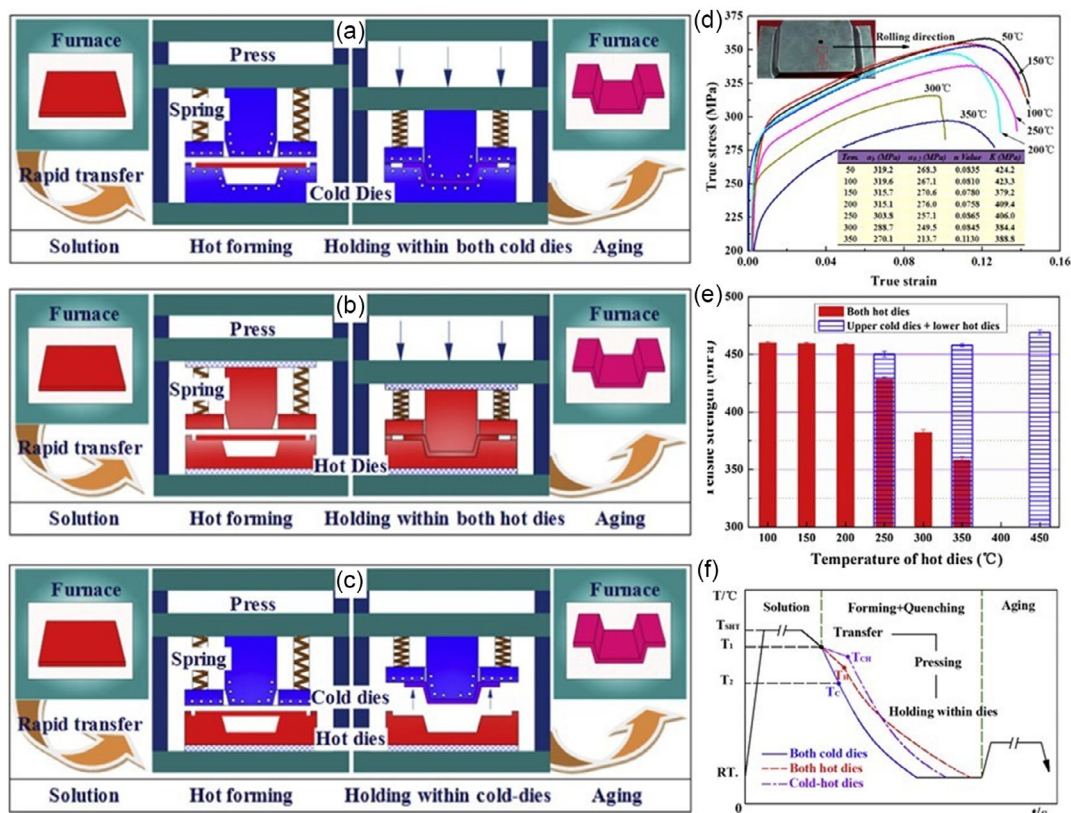


Figure 24. Schematic illustration of the different process variants and strategies with a) cold forming dies, b) heated forming dies, and c) upper cold and lower heated dies. d) Comparison of the mechanical properties of resulting formed parts for different die temperatures and e) using heated upper and lower dies versus upper cold and lower hot dies. f) Temperature–time profile of the strategies investigated with different die temperatures. Adapted with permission.^[170] Copyright 2015, Elsevier.

tensile strength were obtained with decreasing die temperature (ranging from 350 to 50 °C), Figure 24d. From these observations,^[168,169,171] it can be concluded that at lower die temperatures, the precipitation rate decreased due to the high cooling rate and resulting low diffusion rate. Consequently, the supersaturated state was preserved to a higher extent during the forming and quenching step. On the other hand, at higher die temperatures (e.g., 350 °C), the precipitation rate is higher due to faster diffusion. This behavior leads to lower supersaturation after forming and quenching and explains the decrease in precipitation hardness, also observed in other studies.^[85,168]

In order to preserve the required formability on the one hand and to obtain sufficiently high cooling rates on the other, a heated lower die and a cooled upper die have been used simultaneously in other studies^[170,171] (Figure 24c). The heated lower die avoids premature cooling of the blank on first contact during the forming process, while the cooled upper die shows rapid cooling after the complete forming operation. Compared to the approach of heating both dies, this configuration improves the mechanical properties while maintaining an adequate formability (die temperatures of 250, 350, and 450 °C (Figure 24e). SEM and TEM investigations have demonstrated the underlying mechanisms on the microstructural level (Figure 25a–d). For all cooling rates and die configurations investigated, an almost homogeneous distribution of very fine metastable precipitations is observed. The use of heated upper and lower dies caused an increase in the number density of precipitates (Figure 25a 250 °C, b) 350 °C) over and above the heated upper/cooled lower configuration, due to the lower cooling rates and higher diffusion rates. When the die temperature was increased from 250 to 350 °C,

these precipitates increased in size and number (Figure 25b). In contrast to this, forming the blank with lower hot and upper cold dies inhibits the further growth of precipitates, and no coarse precipitate particles are observed (Figure 25c) 250 °C and d) 350 °C).^[170] Due to the higher degree of dislocation and particle interaction and to the PH mechanisms, such microstructures with fine, evenly dispersed precipitates gave improved mechanical strength.^[173,174]

TEM observations illustrate the difference between the microstructures obtained by upper-cooled die quenching, as shown in Figure 25e,f and air quenching, Figure 25g,h, after forming in a heated lower die at 450 °C. Fine lath-shaped (50 nm × 100 nm) and homogeneously distributed metastable precipitates are shown in Figure 25e,f, obtained with an upper-cooled die, whereas with air cooling (Figure 25g,h), coarse needle-shaped precipitates of 750–1000 nm are observed. As a result of the lower cooling rate, air quenching enables higher precipitation and nucleation rates and an increase in size of the precipitates, explaining the resulting decrease in mechanical strength.

Considering the main hardening mechanisms for precipitation-hardenable aluminum alloys explained in Section 2 in the case of thermomechanical process design, precipitate types and morphology play a fundamental role as they contribute most effectively to the overall strength. In another study,^[175] the contribution of precipitate types and distributions on the strengthening of precipitation-hardenable aluminum alloy AA7075 is investigated after solution heat treatment and integrated cooling using cooled forming tools. Isothermal aging (at 120 °C for 24 h is compared with preaging (PA: 180 °C for 5 min) with simulated baking (SB: 180 °C for 30 min). TEM

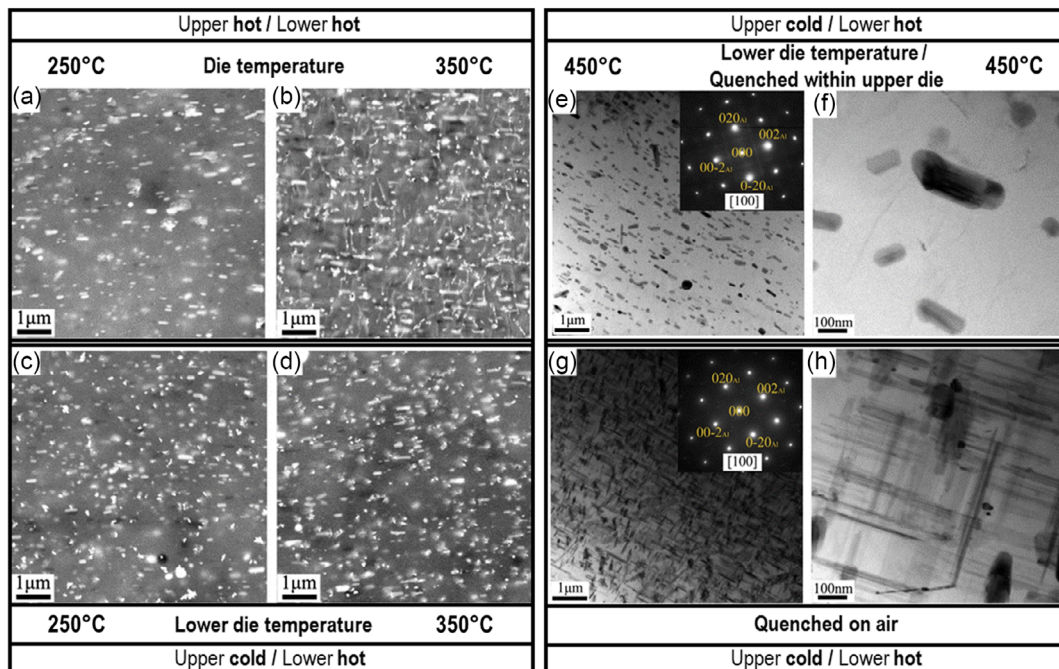


Figure 25. SEM observations of precipitate distribution in the samples formed and quenched using upper and lower hot dies at a) 250 °C and b) 350 °C. Upper cold die with lower hot die at c) 250 °C and d) 350 °C. TEM analysis and SAED patterns of microstructure of formed parts using upper cold and lower hot dies at 450 °C quenched within the e) upper die and f) and air. (g) and (h). Adapted with permission.^[170] Copyright 2015, Elsevier.

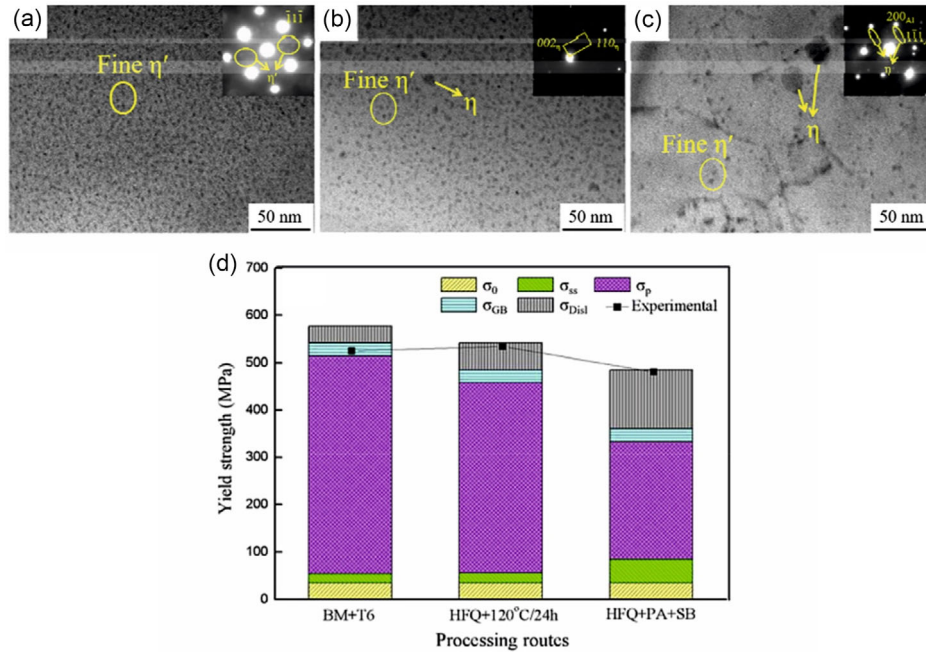


Figure 26. TEM observations of the microstructure of precipitation-hardenable aluminum alloy AA7075: a) as-received base material in T6 condition, b) material isothermally aged at 120 °C for 24 h, c) PA + SB, and d) overall contributions of strengthening mechanisms after thermomechanical treatment. Adapted with permission.^[175] Copyright 2019, Elsevier.

clearly reveals the presence of a different fraction of η' -phase, mainly resulting from the aging processes, from that observed in the T6 condition (BM + T6) (Figure 26a–c). For both aging strategies, the η' -phase and η -phase are observed within the grain structure. In the PA + SB microstructure, however, the volume fraction of the η' -phase is lower and the number density as well as the size of equilibrium η -phase precipitates is higher. Hence, by comparing the overall contributions of the different strengthening mechanisms to YS, it becomes clear that the contribution of precipitation strengthening is higher for the microstructure isothermally aged at 120 °C for 24 h than for the PA + SB condition, mainly due to the presence of fine η' -phase precipitates and their higher volume fraction in the former condition (Figure 26c). For the PA + SB condition, a larger contribution to SSS is associated with the decreased fraction of η' -phase and the consequently higher concentration of the alloying elements Mg and Zn in solid solution.^[175] In addition, the significantly higher contribution from dislocation strengthening in the PA + SB condition is explained in this study by an increase in the strain energy of initially straight dislocations due to bending as they interact with precipitates.^[175] Since the elastic strain energy of a dislocation is proportional to its length, an increase in the length of a moving dislocation as it bows around coarse precipitates results in an increase in its energy. Hence, the line tension T , which is the increase in the energy of a dislocation per unit increase in the length of its line, is given by^[18]

$$T = \alpha Gb^2 \quad (8)$$

where α is a constant, G is the shear modulus, and b is the Burgers vector.

4.1.4. Influences on Aging Treatment in Hot Forming–Quenching

In precipitation-hardenable aluminum alloys, precipitation kinetics are affected by the presence of crystal defects such as vacancies, dislocations, and GBs.^[82,176,177] All these defect types interact on the atomic scale with precipitates, influencing their kinetics of nucleation and of coarsening during aging. The generation of a high dislocation density during hot deformation can therefore influence the final mechanical properties, since dislocations act as fast diffusion paths for solutes, and additionally, interactions between solute and dislocations result in a flux of solute to the dislocations.^[177] As a result, deformation gradients along a component after hot stamping and aging can cause dissimilar mechanical properties.

In another study,^[178] therefore, to emulate an integrated hot stamping process and to determine the influence of defined degrees of deformation on the distribution of final material hardness distribution, hot deformation ranging from 2% to 10% was conducted at 420 °C within a tensile testing machine equipped with a moveable inductor and contact cooling devices after solution heat treatment and prior to artificial aging. The results were then compared to the distribution of the same properties, after artificial aging, of a part formed under industrial conditions using the same process parameters. An inhomogeneous hardness distribution was reported, which was attributed to the cooling conditions of the heated sheet material during the hot stamping operation. No significant increase in hardness in the locally deformed zones, for example in the radii, was found. These observations agreed with the hardness distribution obtained using the emulated thermomechanical process, showing no significant increase in the hardness after hot deformation at 2% or 10%. These phenomena are

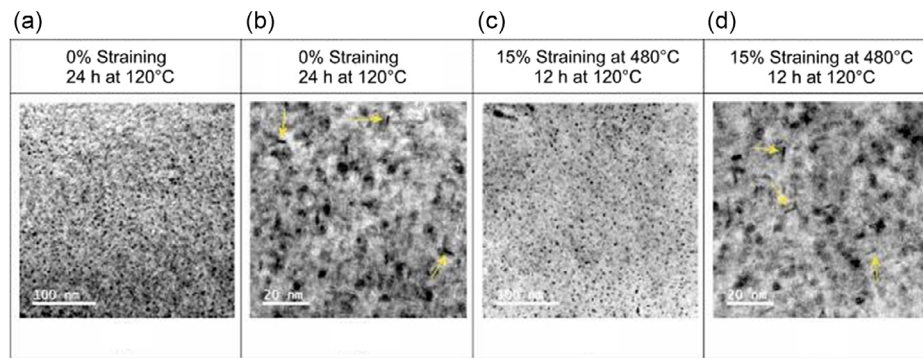


Figure 27. TEM micrographs of aged AA7075 in peak-hardened condition after 0% straining and 15% straining at 480 °C. Reproduced with permission.^[179] Copyright 2018, MDPI.

attributed to the activation of softening mechanisms, such as dynamic recrystallization or recovery, during hot deformation.

In another study,^[179] the microstructural evolution in AA7075 after hot deformation at different degrees of deformation is presented (Figure 27a,b). The material was soaked at 480 °C and strained from 0% to 15%, followed by water quenching to room temperature. The peak hardness was achieved after 24 h of aging at 120 °C for the 0 % strain case, but after only 12 h for 15% straining. In both conditions, homogeneously distributed precipitates were observed after ageing to the respective peak-aged condition. From the TEM observations, it could be seen that the precipitates present in the microstructure were the metastable η' phase. In addition, several elongated ellipsoidal particles were present, which are associated with a higher Cu content (see yellow arrows in Figure 27b,d). The precipitation sequence in Al–Zn–Mg alloys and other heat-treatable aluminum alloys is given in Table 2. In AA7075, GP zones are initially formed, followed by metastable coherent η' , then semicoherent, and stable incoherent η (MgZn_2) precipitates.

4.1.5. Influences on Artificial Aging Treatment

The final mechanical properties of heat-treatable aluminum alloys are obtained during the aging or PH process and depend on the alloying elements and the preserved supersaturation.^[82,180–185] The general aging process and the crystallographic nature of the precipitates has been studied in

a multitude of investigations in the literature.^[186–191] A clear increase in strength after artificial aging with respect to that achieved using natural aging is observed as a result of the different precipitation kinetics and nucleation processes occurring at higher temperatures. Applying thermal as well as mechanical energy accelerates these mechanisms. After nucleation of clusters or highly coherent but metastable precipitates, a sequence of progressively more stable precipitates is formed, until the final thermodynamically stable phase is reached. This final stable phase is usually associated with the overaged condition in which the strength and hardness are lower than those of the peak-aged condition.

As described above, the SSSS condition can be achieved using a high cooling rate after solution heat treatment; in the hot stamping process, this is obtained using cooled forming tools, as reported in other studies.^[159,192–194] The cooling rate over a temperature range of 400 to 290 °C is measured in another study^[194] in the precipitation-hardenable aluminum alloys AA6082 and AA7075 using the novel HFQ hot stamping process. After solution heat treatment, the alloys are cooled with different cooling media, namely 1) water, 2) a water-aquatenside mixture (AQ-D) that allows a high cooling rate and lower thermal distortion than water quenching alone, and 3) cooled forming tools (Figure 28a,b). The highest cooling rate, of higher than 1000 °C s⁻¹, is achieved in water. The water + aquatenside mixture gives an intermediate rate and the cooled forming tools give the lowest cooling rate of 493 °C s⁻¹.

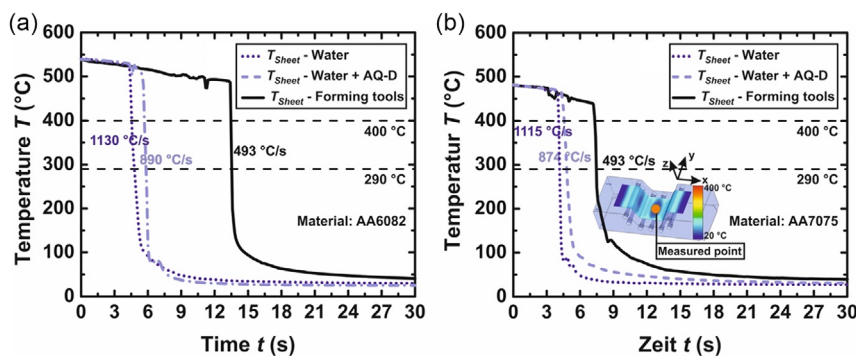


Figure 28. Cooling rate obtained after solution heat treatment using different processes for precipitation-hardenable aluminum alloys: a) AA6082 and b) AA7075.

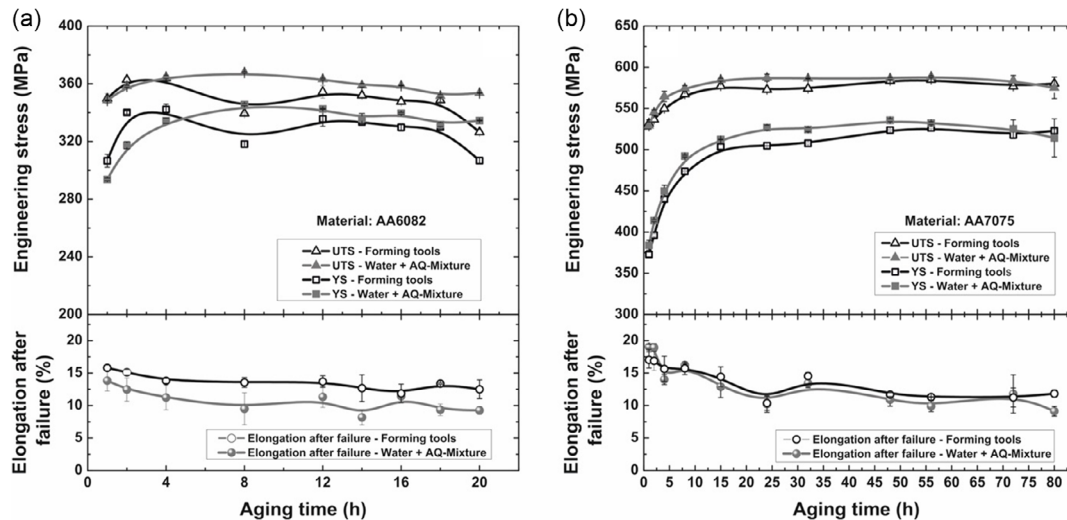


Figure 29. Influence of cooling strategy and aging parameters on mechanical properties of AA6082 and AA7075 after artificial aging. Reproduced with permission.^[195] Copyright 2019, Wissenschaftliche Skripten.

The mechanical properties of material formed and quenched using cooled forming tools are compared in other studies^[194,195] to those quenched using the water + aquatensite mixture (AG-D) after artificial aging with different parameters (Figure 29a,b) to determine the abilities of these techniques to maintain an SSSS state after quenching and to give high final material strength values. From this figure it is clear that the YS and UTS obtained using different cooling strategies are very similar and do not vary greatly with aging time. The addition of another process step, or subsequent thermal processing, is therefore not required for the achievement of the desired mechanical properties.

Experimental results obtained in another study^[158] show that after subsequent aging, the integrated HFQ process gives a product with almost the same mechanical properties as conventional forming. The potential for accelerating the aging process in precipitation-hardenable aluminum alloy AA6082 is demonstrated in another study,^[163] where the aim was to obtain mechanical properties comparable to those in the T6 condition. In the first step, the material was heated, over a period of 15 min, to the target aging temperature of 220 °C and held isothermally for 5 min. In the second step, the material was heated to 180 °C for 30 min to simulate a paint-bake process, which usually takes place in the automotive production line. The total processing time of about 1 h presented in another study^[163] reveals the potential for reduction in processing time with respect to the conventional aging process, while achieving almost the same mechanical properties as a T6 temper. Hence, it can be concluded from the investigations discussed here that the proposed thermomechanical process^[14,53,196,197] using cooled-forming tools enables the attainment of high material strength after artificial aging comparable to that achievable in the T6 condition.

5. Summary and Conclusions

This review has presented several forming strategies which have been developed with the aim of improving the formability of

high-strength, lightweight materials such as heat-treatable wrought aluminum alloys. Based on the results existing in the literature and presented in the review, the following conclusions can be drawn.

Lightweighting is an important issue for environmental reasons, particularly in the automotive sector. There is strong motivation to replace steel components with high-strength aluminum for reasons of energy efficiency, whilst maintaining a high level of passenger safety. High-strength aluminum alloys are suited to this application thanks to their low density and high strength-to-weight ratio and have already found application in electric vehicles leading to a higher range. Concerning the use of high-strength aluminum alloys in electric car bodies, the key element is the continuous reduction of vehicle weight, which is directly linked to an increase in travel distance per battery charge; this is in addition to any increase in range, thanks to increases in battery charging capacities. High-strength aluminum alloys exhibit an aptitude for being processed within a defined and robust forming route as well as suitability for application as structural components. Thus, the use of this class of alloys with durable and optimized forming processes is a solution for modern mass production in the automotive industry.

Aluminum alloys have four main strengthening mechanisms; the highest strengths can be achieved in age-hardenable alloys thanks to the formation of second-phase precipitates. The heat treatment cycle of age-hardenable aluminum alloys comprises solution heat treatment to dissolve the alloying elements, fast cooling (quenching) to room temperature to obtain a SSSS, and artificial aging at moderate temperature to obtain the precipitate phases that provide strengthening. Hence, the final mechanical properties of age-hardenable aluminum alloys depend strongly on composition and heat treatment parameters.

Age-hardenable aluminum alloys have low formability at room temperature in their peak-aged conditions, suffering from springback and poor dimensional accuracy. Therefore, strategies have been developed to improve the formability of these alloys while benefiting from the excellent final mechanical properties.

Each of these has been developed to take advantage of the microstructural mechanisms underlying the strengthening behavior of aluminum alloys.

WT forming enables the manufacture of complex structures for the automotive industry by applying an integrated forming step directly after rapid quenching to room temperature. The desired mechanical properties can be subsequently achieved after the forming step during artificial aging. However, a limitation of this technique is the propagation of surface phenomena, known as shear bands, during plastic deformation at low temperature. These degrade the surface quality. WT forming is a technique for forming high-strength aluminum alloys to achieve complex-shaped geometries such as car body structures. By forming at high deformation rates, it is possible to suppress the appearance of the PLC effect due to a lower degree of interaction between dislocations and solute atoms within the grain structure at these deformation rates. However, due to the high dislocation density generated at room temperature in the formed zones during the deformation step, inhomogeneities in material strength may be generated after the aging treatment. These occur because of the increased precipitate nucleation and growth induced by the high density of dislocations in the deformed zones.

Alternative approaches to extend the limits of aluminum alloys are superplastic and quick forming. The forming step for both techniques take place at temperatures higher than the solution heat treatment temperature. The main advantage of these techniques is their capability to shape complex geometries, due to the increase in formability that they confer at high temperatures.

The most promising of the new approaches to the forming of high-strength aluminum alloys appears to be the HFQ method, which integrates the heat treatment into the forming process. This gives almost the same mechanical properties as in the T6 condition with a high dimensional accuracy. The innovation of this approach is the combination of the shaping step at high temperature with the required quenching from the solution annealing temperature before the final aging process. The dies used in this process have two functions: (1) defining the final shape and (2) cooling the material. The main advantage conferred is a shorter process time and the energy-efficient integration of the hot forming process. Much research has been conducted on the optimization of process parameters such as heating rates, solution annealing temperatures, and soaking times as well as tool heating and cooling strategies and aging parameters, to minimize the total cycle time while obtaining excellent mechanical properties in the final parts. These studies demonstrate that the new hot forming–quenching process can produce parts with properties that are almost the same as those formed by conventional forming processes, with reduced production times and cost savings. However, there is still potential for increasing the efficiency in each process stage. In addition, the effect of differential cooling, as proposed for high-strength steel,^[198,199] on precipitation-hardenable aluminum alloys using this novel forming process should be considered.^[200,201]

Acknowledgements

E.S. would like to thank the Hessen State Ministry for Higher Education, Research and the Arts, Initiative for the Development of Scientific and Economic Excellence (LOEWE) for financial support of the special research

project “ALLEGRO.” V.Y. and J.L. would like to thank EPSRC for financial support from grant no. EP/R001715/1 “Lightform: Embedding Materials Engineering in Manufacturing with Light Alloys.”

Open Access funding enabled and organized by Projekt DEAL.

Conflict of Interest

The authors declare no conflict of interest.

Keywords

high-strength aluminum alloys, hot stamping, precipitation hardening, thermomechanical processes, warm forming

Received: January 30, 2023

Revised: April 13, 2023

Published online: June 29, 2023

- [1] K. Steinhoff, in *Proc. of the 1st Inter. Seminar on Hot Sheet Metal Forming of High-Performance Steel* (Eds: K. Steinhoff, M. Oldenburg, B. Prakash), Wissenschaftliche Skripten, Kassel (GER) **2010**.
- [2] K. Steinhoff, N. Saba, M. Maikranz-Valentin, U. Weidig, in *Proc. of the 2nd Inter. Conf. on Hot Sheet Metal Forming of High-Performance Steel, Auerbach (D)* (Eds: K. Steinhoff, M. Oldenburg, B. Prakash), Wissenschaftliche Skripten, Luleå (SWE) **2009**.
- [3] M. Raugei, O. El, L. Wang, J. Lin, D. Morrey, *J. Clean. Prod.* **2014**, *83*, 80.
- [4] H. Monteiro, R. Alonso, M. Gonçalves, M. Iten, N. S. Caetano, *Energy Rep.* **2022**, *8*, 241.
- [5] E. A. Starke, Y. Khalfalla, K. Y. Benyounis, *Ref. Modul. Mater. Sci. Mater. Eng.* **2016**, 118, <https://doi.org/10.1016/B978-0-12-803581-8.03376-2>.
- [6] W. S. Miller, L. Zhuang, J. Bottema, A. Wittebrood, P. De Smet, A. Haszler, A. Vieregge, *Mater. Sci. Eng. A* **2000**, *280*, 37.
- [7] G. Anya odor, C. Koroschetz, *J. Phys.: Conf. Series*, **2017**, *896*, 012093.
- [8] Y. Liu, L. Wang, B. Zhu, Y. Wang, Y. Zhang, *Proc. Manuf.* **2018**, *15*, 701.
- [9] Z. Yue, X. Chu, J. Gao, *Procedia Manuf.* **2018**, *15*, 716.
- [10] M. Merklein, M. Johannes, M. Lechner, A. Kuppert, *J. Mater. Process. Technol.* **2014**, *214*, 151.
- [11] M. Teller, I. Ross, A. Temmler, R. Poprawe, S. Prünte, J. M. Schneider, G. Hirt, *Key Eng. Mater.* **2018**, *767*, 189.
- [12] L. Deng, X. Wang, J. Jin, L. Xia, *Procedia Eng.* **2017**, *207*, 2388.
- [13] J. Yanagimoto, K. Oyamada, T. Nakagawa, *CIRP Ann.* **2005**, *54*, 213.
- [14] J. Lin, T. A. Dean, A. D. Foster, L. Wang, D. Balint, *WO2011/058332A1*, **2010**.
- [15] A. D. Foster, T. A. Dean, J. Lin, *WO 2010/032002 A1*, **2008**.
- [16] G. E. Totten, D. S. MacKenzie, *Choice Rev. Online* **2004**, *41*, 41.
- [17] E. Hornbogen, *J. Light Met.* **2001**, *1*, 127.
- [18] D. Hull, D. J. Bacon, *Introduction To Dislocations*, Elsevier Ltd., Amsterdam **2011**.
- [19] D. Raabe, M. Sachtler, H. Weiland, G. Scheele, Z. Zhao, *Acta Mater.* **2003**, *51*, 1539.
- [20] Z. Hu, H. Zhang, H. Zhu, Z. Xiao, X. Nie, X. Zeng, *Mater. Sci. Eng. A* **2019**, *759*, 154.
- [21] R. E. Sanders, S. F. Baumann, H. C. Stumpf, *Treatise Mater. Sci. Technol.* **1989**, *31*, 65.
- [22] M. Dixit, R. S. Mishra, K. K. Sankaran, *Mater. Sci. Eng. A* **2008**, *478*, 163.

- [23] J. A. Wert, N. E. Paton, C. H. Hamilton, M. W. Mahoney, *Metall. Trans. A, Phys. Metall. Mater. Sci.* **1981**, 12A, 1267.
- [24] E. O. Hall, *Proc. Phys. Soc. Sect. B* **1951**, 64, 747.
- [25] X. Jin, P. Zhao, W. Chen, K. Ma, Y. Fu, S. Guo, D. Feng, *J. Mater. Eng. Perf.* **2022**, 31, 10354.
- [26] E. Arzt, *Acta Mater.* **1998**, 46, 5611.
- [27] U. F. Kocks, H. Mecking, *Prog. Mater. Sci.* **2003**, 48, 171.
- [28] G. Fribourg, Y. Bréchet, A. Deschamps, A. Simar, *Acta Mater.* **2011**, 59, 3621.
- [29] J. Courbon, J. L. Duval, *Le J. Phys. IV* **1993**, 03, C7.
- [30] A. Deschamps, M. Niewczas, F. Bley, Y. Brechet, J. D. Embury, L. Le Sinq, F. Livet, J. P. Simon, *Philos. Mag. A* **1999**, 79, 2485.
- [31] A. P. Mouritz, *Introduction To Aerospace Materials*, Elsevier, Amsterdam **2012**.
- [32] U. Messerschmidt, M. Bartsch, *Mater. Chem. Phys.* **2003**, 81, 518.
- [33] A. Kelly, R. Nicholson, *Strengthening Methods In Crystals*, Elsevier, Amsterdam **1971**.
- [34] G. Gottstein, *Materialwissenschaft Und Werkstofftechnik*, Springer Berlin Heidelberg, Berlin, Heidelberg **2015**.
- [35] E. Hornbogen, H. Warlimont, in *Metallkunde*, Springer Berlin Heidelberg, Berlin, Heidelberg **2001**, pp. 60–81.
- [36] E. Hornbogen, G. Eggeler, E. Werner, *Aufbau Und Eigenschaften Von Keramik-, Metall-, Polymer- Und Verbundwerkstoffen*, Springer-Verlag Berlin Heidelberg, Berlin, Heidelberg **2012**.
- [37] L. K. Berg, J. Gjøannes, V. Hansen, X. Z. Li, M. Knutson-Wedel, G. Waterloo, D. Schryvers, L. R. Wallenberg, *Acta Mater.* **2001**, 49, 3443.
- [38] J. Buha, R. N. Lumley, A. G. Crosky, *Mater. Sci. Eng. A* **2008**, 492, 1.
- [39] Z. Chen, K. Yan, C. Ren, S. Naseem, *J. Alloys Compd.* **2021**, 875, 159950.
- [40] G. Sha, A. Cerezo, *Acta Mater.* **2004**, 52, 4503.
- [41] J. Chen, L. Zhen, S. Yang, W. Shao, S. Dai, *Mater. Sci. Eng. A* **2009**, 500, 34.
- [42] M. Liu, B. Klobes, K. Maier, *Scr. Mater.* **2011**, 64, 21.
- [43] J. Z. Liu, J. H. Chen, X. B. Yang, S. Ren, C. L. Wu, H. Y. Xu, J. Zou, *Scr. Mater.* **2010**, 63, 1061.
- [44] J. Gjøannes, C. J. Simensen, *Acta Metall.* **1970**, 18, 881.
- [45] Y. Y. Li, L. Kovarik, P. J. Phillips, Y. F. Hsu, W. H. Wang, M. J. Mills, *Philos. Mag. Lett.* **2012**, 92, 166.
- [46] T. F. Chung, Y. L. Yang, B. M. Huang, Z. Shi, J. Lin, T. Ohmura, J. R. Yang, *Acta Mater.* **2018**, 149, 377.
- [47] W. Yang, S. Ji, M. Wang, Z. Li, *J. Alloys Compd.* **2014**, 610, 623.
- [48] R. A. Ayres, *Metall. Trans. A* **1977**, 8, 487.
- [49] G. L'Esperance, W. Roberts, M. Loreto, D. Wilson, *12th Biennial Congress Inte. Deep Drawing Research Group*, S. Margherita Ligure, Italy May 24–28 **1982**.
- [50] D. Li, A. K. Ghosh, *J. Mater. Process. Technol.* **2004**, 145, 281.
- [51] L. Schell, M. Emele, A. Holzbeck, P. Groche, *Tribol. Int.* **2022**, 168, 107449.
- [52] X. Liu, O. El Fakir, Y. Zheng, M. M. Gharbi, L. L. Wang, *Int. J. Heat Mass Transf.* **2019**, 137, 74.
- [53] K. Zheng, Y. Dong, D. Zheng, J. Lin, T. A. Dean, *J. Mater. Process. Technol.* **2018**, 268, 87.
- [54] K. Zheng, D. J. Politis, J. Lin, T. A. Dean, *Int. J. Mech. Sci.* **2016**, 110, 138.
- [55] N. Bay, *J. Mater. Process. Technol.* **1997**, 71, 76.
- [56] D. Carle, G. Blount, *Mater. Des.* **1999**, 20, 267.
- [57] E. S. de Argandoña, L. Galdos, R. Ortubay, J. Mendiguren, X. Agirretxe, *Key Eng. Mater.* **2015**, 651–653, 199.
- [58] K. Zheng, D. J. Politis, L. Wang, J. Lin, *Int. J. Light. Mater. Manuf.* **2018**, 1, 55.
- [59] J. Glazer, S. L. Verzasconi, R. R. Sawtell, J. W. Morris, *Metall. Trans. A* **1987**, 18, 1695.
- [60] S. H. Zhang, J. Danckert, *J. Mater. Process. Technol.* **1998**, 83, 14.
- [61] L. Lang, J. Danckert, K. B. Nielsen, *Int. J. Mach. Tools Manuf.* **2004**, 44, 649.
- [62] B. T. Araghi, G. L. Manco, M. Bambach, G. Hirt, *CIRP Ann.* **2009**, 58, 225.
- [63] K. Jawale, J. F. Duarte, A. Reis, M. B. Silva, *Int. J. Solids Struct.* **2018**, 151, 145.
- [64] P. A. F. Martins, N. Bay, M. Skjoedt, M. B. Silva, *CIRP Ann.* **2008**, 57, 247.
- [65] S. B. M. Echraf, M. Hrairi, *Mater. Manuf. Process.* **2011**, 26, 1404.
- [66] F. Grabner, J. A. Österreicher, B. Gruber, N. Papenberg, F. Gerstner, S. Kirmstötter, C. M. Schlögl, *Adv. Eng. Mater.* **2019**, 21, 1900089.
- [67] B. Gruber, F. Grabner, G. Falkinger, A. Schökel, F. Spieckermann, P. J. Uggowitzer, S. Pogatscher, *Mater. Des.* **2020**, 193, 108819.
- [68] J. Lee, H. J. Bong, D. Kim, Y. S. Lee, Y. Choi, M. G. Lee, *JOM J. Minerals Metals Mater. Soc.* **2019**, 71, 4393.
- [69] K. Nakazima, T. Kikuma, K. Hasuka, *Yamata Tech. Rep.* **1968**, 264, 8517.
- [70] S. Entesari, A. Abdollah-zadeh, N. Habibi, A. Mehri, *J. Manuf. Process.* **2017**, 29, 74.
- [71] N. Jia, P. Eisenlohr, F. Roters, D. Raabe, X. Zhao, *Acta Mater.* **2012**, 60, 3415.
- [72] D. Dorner, S. Zaefferer, D. Raabe, *Acta Mater.* **2007**, 55, 2519.
- [73] J. Z. Chen, L. Zhen, L. W. Fan, S. J. Yang, S. L. Dai, W. Z. Shao, *Trans. Nonferrous Met. Soc. China* **2009**, 19, 1071.
- [74] H. Halim, D. S. Wilkinson, M. Niewczas, *Acta Mater.* **2007**, 55, 4151.
- [75] N. Tian, G. Wang, Y. Zhou, K. Liu, G. Zhao, L. Zuo, *Materials (Basel)*. **2018**, 11, 1533.
- [76] A. Yilmaz, *Sci. and Technol. of Adv. Mater.* **2011**, 12, 16.
- [77] Y. Choi, J. Lee, H. J. Bong, M. G. Lee, *Met. Mater. Int.* **2022**, 29, 157.
- [78] J. Günzel, J. Hauß, P. Groche, *IOP Conf. Ser. Mater. Sci. Eng.* **2021**, 1157, 012086.
- [79] T. Cheng, X. Xu, Y. Cai, S. Fu, Y. Gao, Y. Su, Y. Zhang, Q. Zhang, *Opt. Lasers Eng.* **2015**, 65, 89.
- [80] H. Aboulfadl, J. Deges, P. Choi, D. Raabe, *Acta Mater.* **2015**, 86, 34.
- [81] C. B. Fuller, M. W. Mahoney, M. Calabrese, L. Miconi, *Mater. Sci. Eng. A* **2010**, 527, 2233.
- [82] S. Pogatscher, H. Antrekowitsch, H. Leitner, T. Ebner, P. J. Uggowitzer, *Acta Mater.* **2011**, 59, 3352.
- [83] J. Banhart, C. S. T. Chang, Z. Liang, N. Wanderka, M. D. H. Lay, A. J. Hill, *Adv. Eng. Mater.* **2010**, 12, 559.
- [84] J. Min, F. Xie, Y. Liu, Z. Hou, J. Lu, J. Lin, *CIRP J. Manuf. Sci. Technol.* **2022**, 37, 11.
- [85] E. Scharifi, U. Savaci, Z. B. Kavaklioglu, U. Weidig, S. Turan, K. Steinhoff, *Mater. Charact.* **2021**, 174, 111026.
- [86] J. W. Gibbs, *The Collected Works of J. Willard Gibbs*, Yale University Press, New Haven CT (USA) **1948**.
- [87] E. Scharifi, D. Kuhnhehn, A. Ademaj, U. Weidig, in *6th Inter. Conf. Hot Steel Metal Forming of High-Performance Steel, CHS2 2017- Proceedings* (Eds.: K. Steinhoff, M. Oldenburg, B. Prakash), Atlanta, GA, **2017**.
- [88] M. Vrolijk, C. Koroschetz, M. Holecck, K. E. Snilsberg, L.-O. Jönsson, G. Anyasodor, D. Lorenz, in *6th Inter. Seminar on Hot Sheet Metal Forming of High-Performance Steel CHS2* (Eds.: K. Steinhoff, M. Oldenburg, B. Prakash), Atlanta, GA.
- [89] H. Gleiter, E. Hornbogen, G. Ro, *Acta Metall.* **1968**, 16, 1053.
- [90] D. Raabe, D. Ponge, R. Kirchheim, H. Assadi, Y. Li, S. Goto, A. Kostka, M. Herbig, S. Sandl, M. Kuzmina, J. Millán, L. Yuan, P. P. Choi, *Microstructural Design Of Advanced Engineering Materials*, Wiley-VCH Verlag GmbH & Co. KGaA, Weinheim, Germany **2013**, pp. 267–298.
- [91] D. Raabe, M. Herbig, S. Sandlöbes, Y. Li, D. Tytko, M. Kuzmina, D. Ponge, P.-P. Choi, *Curr. Opin. Solid State Mater. Sci.* **2014**, 18, 253.

- [92] R. Z. Valiev, N. A. Krasilnikov, N. K. Tsenev, *Mater. Sci. Eng. A* **1991**, 137, 35.
- [93] A. K. Ghosh, C. H. Hamilton, *Metall. Trans. A* **1982**, 13, 733.
- [94] R. Grimes, M. J. Stowell, B. M. Watts, *Met. Technol.* **1976**, 3, 154.
- [95] J. R. Davis, A. I. H. Committee, *ASM Int.* **1993**, 14, 483.
- [96] Y. Murakoshi, M. Takahashi, T. Sano, K. Hanada, H. Negishi, *J. Mater. Process. Technol.* **1998**, 80–81, 695.
- [97] T. Ishikawa, N. Yukawa, K. Suzuki, Y. Suzuki, T. Jimma, *J. Mater. Process. Technol.* **1997**, 68, 236.
- [98] M. Merklein, M. Lechner, A. Kuppert, *Prod. Eng.* **2012**, 6, 541.
- [99] P. F. Bariani, S. Bruschi, A. Ghiotti, F. Michieletto, *CIRP Ann. - Manuf. Technol.* **2013**, 62, 251.
- [100] M. Y. Lee, S. M. Sohn, C. Y. Kang, D. W. Suh, S. Y. Lee, *J. Mater. Process. Technol.* **2004**, 155–156, 1337.
- [101] I. Torca, A. Aginagalde, J. A. Esnaola, L. Galdos, Z. Azpilgain, C. Garcia, *Key Eng. Mater.* **2009**, 423, 105.
- [102] L. Wang, M. Strangwood, D. Balint, J. Lin, T. A. Dean, *Mater. Sci. Eng. A* **2011**, 528, 2648.
- [103] N. Li, M. S. Mohamed, J. Cai, J. Lin, D. Balint, T. A. Dean, *AIP Conf. Proc.* **2011**, 1353, 1555.
- [104] H. Gao, T. Weng, J. Liu, C. Li, Z. Li, L. Wang, *MATEC Web Conf.* **2015**, 21, 05007.
- [105] H. Laurent, J. Coër, R. Grèze, P. Y. Manach, A. Andrade-Campos, M. C. Oliveira, L. F. Menezes, *ISRN Mech. Eng.* **2011**, 2011, 1.
- [106] H. S. Kim, M. Koç, *J. Mater. Process. Technol.* **2008**, 204, 370.
- [107] M. Kumar, N. Sotirov, C. M. Chimani, *J. Mater. Process. Technol.* **2014**, 214, 1769.
- [108] S. Mahabunphachai, M. Koç, *Mater. Des.* **2010**, 31, 2422.
- [109] S. Polak, P. Kaczyński, Z. Gronostajski, K. Jaskiewicz, J. Krawczyk, M. Skwarski, M. Zwierzchowski, W. Chorzępa, *Procedia Eng.* **2017**, 207, 2399.
- [110] W. Huo, L. Hou, Y. Zhang, J. Zhang, *Mater. Sci. Eng. A* **2016**, 675, 44.
- [111] P. L. Wang, H. T. Jiang, R. J. Zhang, S. Y. Huang, *Mater. Sci. Forum* **2016**, 877, 340.
- [112] M. Kumar, N. G. Ross, *Adv. Mater. Sci. Eng.* **2017**, 2017, <https://doi.org/10.1155/2017/7679219>.
- [113] M. Zhao, Y. Xing, Z. Jia, Q. Liu, X. Wu, *J. Alloys Compd.* **2016**, 686, 312.
- [114] R. Hill, *J. Mech. Phys. Solids* **1990**, 38, 405.
- [115] K. Shojaei, S. V. Sajadifar, G. G. Yapici, *Mater. Sci. Eng. A* **2016**, 670, 81.
- [116] S. V. Sajadifar, E. Scharifi, U. Weidig, K. Steinhoff, T. Niendorf, *Metals* **2020**, 10, 1.
- [117] H. Zhang, G. Chen, Q. Chen, F. Han, Z. Zhao, *J. Alloys Compd.* **2018**, 743, 283.
- [118] H. J. McQueen, J. E. Hockett, *Metall. Trans.* **1970**, 1, 2997.
- [119] H. J. McQueen, N. D. Ryan, *Mater. Sci. Eng. A* **2002**, 322, 43.
- [120] J. Decke, A. Engelhardt, L. Rauch, S. Degener, S. V. Sajadifar, E. Scharifi, K. Steinhoff, T. Niendorf, B. Sick, *Crystals* **2022**, 12, 1281.
- [121] S. K. Paul, *Comput. Mater. Sci.* **2012**, 65, 91.
- [122] M. Rajamuthamilselvan, S. Ramanathan, *J. Alloys Compd.* **2011**, 509, 948.
- [123] R. K. Gupta, V. Anil Kumar, A. Sarath Krishnan, J. Niteshraj, *J. Mater. Eng. Perform.* **2019**, 28, 5021.
- [124] S. Mandal, M. Jayalakshmi, A. K. Bhaduri, V. Subramanya Sarma, *Metall. Mater. Trans. A Phys. Metall. Mater. Sci.* **2014**, 45, 5645.
- [125] M. Taheri-Mandarjani, A. Zarei-Hanzaki, H. R. Abedi, *Mater. Sci. Eng. A* **2015**, 637, 107.
- [126] H. Yamagata, *Scr. Metall. Mater.* **1992**, 27, 727.
- [127] J. Lv, J.-H. Zheng, V. A. Yardley, Z. Shi, J. Lin, *Metals* **2020**, 10, 1516.
- [128] D. Raabe, *Phys. Metall. Fifth Ed.* **2014**, 1, 2291.
- [129] M. R. Rokni, A. Zarei-Hanzaki, A. A. Roostaei, H. R. Abedi, *Mater. Des.* **2011**, 32, 2339.
- [130] E. Cerri, E. Evangelista, A. Forcellese, H. J. McQueen, *Mater. Sci. Eng. A* **1995**, 197, 181.
- [131] Y. C. Lin, H. Yang, D. G. He, J. Chen, *Mater. Des.* **2019**, 183, 108122.
- [132] H. J. McQueen, C. A. C. Imbert, *J. Alloys Compd.* **2004**, 378, 35.
- [133] H. J. McQueen, S. Spigarelli, M. E. Kassner, E. Evangelista, *Hot Deformation And Processing Of Aluminum Alloys*, CRC Press, Boca Raton, FL **2011**.
- [134] E. Scharifi, J. A. Nietsch, A. Quadfasel, U. Weidig, K. Steinhoff, *Metals* **2022**, 12, 1609.
- [135] J. J. Jonas, X. Quelelennec, L. Jiang, É. Martin, *Acta Mater.* **2009**, 57, 2748.
- [136] A. Najafzadeh, J. J. Jonas, *ISIJ Int.* **2006**, 46, 1679.
- [137] P. A. Friedman, S. G. Luckey, W. B. Copple, R. Allor, C. E. Miller, C. Young, *J. Mater. Eng. Perform.* **2004**, 13, 670.
- [138] Y. Luo, S. G. Luckey, P. A. Friedman, Y. Peng, *Int. J. Mach. Tools Manuf.* **2008**, 48, 1509.
- [139] T. G. Nieh, J. Wadsworth, *Mater. Sci. Forum* **1994**, 170–172, 359.
- [140] T. G. Nieh, J. Wadsworth, *Mater. Sci. Eng. A* **1991**, 147, 129.
- [141] S. R. Babu, S. Deivanayagam, M. Aravind, *Procedia Eng.* **2014**, 97, 1379.
- [142] A. J. Barnes, *Mater. Sci. Forum* **1994**, 170–172, 701.
- [143] J. Pilling, B. Geary, N. Ridley, **1986**.
- [144] A. A. Tavassoli, S. E. Razavi, N. M. Fallah, *Metall. Trans. A* **1975**, 6, 591.
- [145] G. Luckey Jr., P. Friedman, K. Weinmann, *J. Mater. Process. Technol.* **2009**, 209, 2152.
- [146] P. E. Krajewski, J. G. Schroth, *Superplast. Form. Adv. Met. Mater.* **2011**, 272, <https://doi.org/10.1533/9780857092779.3.272>.
- [147] P. E. Krajewski, J. G. Schroth, *Mater. Sci. Forum* **2007**, 551–552, 3.
- [148] R. Boissiere, S. Terzi, J. J. Blandin, L. Salvo, in *EuroSPF08, HAL Open Science, Carcassonne, (FRA)* **2008**, 1.
- [149] R. P. Garrett, J. Lin, T. A. Dean, *Int. J. Plast.* **2005**, 21, 1640.
- [150] R. P. Garrett, J. Lin, T. A. Dean, *Adv. Mater. Res.* **2005**, 6–8, 673.
- [151] M. Mohamed, J. Lin, A. Foster, T. Dean, J. Dear, *Procedia Eng.* **2014**, 81, 1689.
- [152] J. Zhou, B. Wang, J. Lin, L. Fu, *Arch. Civ. Mech. Eng.* **2013**, 13, 401.
- [153] J. Zhou, B. Wang, J. Lin, L. Fu, W. Ma, *Trans. Nonferrous Met. Soc. China* **2014**, 24, 3611.
- [154] T. Maeno, K. Ichiro Mori, R. Yachi, *CIRP Ann. Manuf. Technol.* **2017**, 66, 269.
- [155] J. Lin, D. A. Trevor, G. P. Richard, F. D. Alistair, *Process for Forming Metal Alloy Sheet Components* **2008**, <https://patents.google.com/patent/WO2008059242A2/en>.
- [156] O. El Fakir, L. Wang, D. Balint, J. P. Dear, J. Lin, T. A. Dean, *Int. J. Mach. Tools Manuf.* **2014**, 87, 39.
- [157] A. A. Camberg, F. Bohner, J. Tölle, A. Schneidt, S. Meiners, T. Tröster, *IOP Conf. Ser. Mater. Sci. Eng.* **2018**, 418, 012018.
- [158] D. H. Ko, J. H. Kim, C. J. Lee, D. C. Ko, B. M. Kim, *Trans. Korean Soc. Mech. Eng. A* **2013**, 37, 483.
- [159] A. Wang, K. Zhong, O. El Fakir, J. Liu, C. Sun, L. L. Wang, J. Lin, T. A. Dean, *Int. J. Adv. Manuf. Technol.* **2017**, 89, 1339.
- [160] D. C. Ko, D. H. Ko, J. H. Kim, J. H. Park, *Adv. Mech. Eng.* **2017**, 9, 1.
- [161] A. Foster, D. Szegda, J. Sellors, *MATEC Web Conf.* **2015**, 21, 05014.
- [162] M. Mohamed, N. Li, L. Wang, O. E. Fakir, J. Lin, T. Dean, J. Dear, *MATEC Web Conf.* **2015**, 21, 2.
- [163] N. Li, J. Zheng, C. Zhang, K. Zheng, J. Lin, T. A. Dean, *MATEC Web Conf.* **2015**, 21, 05015.
- [164] Y. Cheng, *J. Mater. Sci. Eng.* **2012**, 01, 1.
- [165] P. Shanmugasundaram, A. K. Dahle, *Encyclopedia of Materials: Science and Technology* **2001**, pp. 111–113.
- [166] S. Shivkumar, S. Ricci, C. Keller, D. Apelian, *J. Heat Treat.* **1990**, 8, 63.
- [167] E. Scharifi, R. Knoth, U. Weidig, *Procedia Manuf.* **2019**, 29, 481.

- [168] X. Fan, Z. He, S. Yuan, K. Zheng, *Mater. Sci. Eng. A* **2013**, 573, 154.
- [169] X. Fan, Z. He, S. Yuan, P. Lin, *Mater. Sci. Eng. A* **2013**, 587, 221.
- [170] X. Fan, Z. He, K. Zheng, S. Yuan, *Mater. Des.* **2015**, 83, 557.
- [171] S. J. Yuan, X. B. Fan, Z. Bin He, in *Procedia Engineering*, Elsevier, Amsterdam **2014**.
- [172] S. V. Sajadifar, E. Scharifi, U. Weidig, K. Steinhoff, T. Niendorf, *HTM J. Heat Treat. Mater.* **2020**, 75, 177.
- [173] J. Hirsch, T. Al-Samman, *Acta Mater.* **2013**, 61, 818.
- [174] P. B. Hirsch, J. Silcix, R. E. Smallmann, K. H. Westmacott, *Philos. Mag.* **1958**, 8, 897.
- [175] Y. F. Jiang, H. Ding, M. H. Cai, Y. Chen, Y. Liu, Y. S. Zhang, *Mater. Charact.* **2019**, 158, 109967.
- [176] F. Schmid, P. Dumitraschkewitz, T. Kremmer, P. J. Uggowitzer, R. Tosone, S. Pogatscher, *Commun. Mater.* **2021**, 2, 1.
- [177] A. Deschamps, F. Livet, Y. Brechet, *Acta Metall.* **1999**, 47, 281.
- [178] E. Scharifi, D. Shoshmina, S. Biegler, U. Weidig, K. Steinhoff, *Metals* **2021**, 11, 681.
- [179] S. H. Jung, J. Lee, M. Kawasaki, *Metals* **2018**, 8, 137.
- [180] C. H. Liu, X. M. Zhang, J. G. Tang, X. X. Liu, L. Chen, *Trans. Nonferrous Met. Soc. China* **2014**, 24, 2289.
- [181] M. S. Remøe, K. Marthinsen, I. Westermann, K. Pedersen, J. Røyset, C. Marioara, *Mater. Sci. Eng. A* **2017**, 693, 60.
- [182] K. Buchanan, K. Colas, J. Ribis, A. Lopez, J. Garnier, *Acta Mater.* **2017**, 132, 209.
- [183] M. W. Zandbergen, Q. Xu, A. Cerezo, G. D. W. Smith, *Acta Mater.* **2015**, 101, 136.
- [184] J. M. Papazian, *Metall. Trans. A* **1981**, 12, 269.
- [185] E. Hornbogen, A. K. Mukhopadhyay, E. A. Starke, *Scr. Metall. Mater.* **1992**, 27, 733.
- [186] J. W. Martin, *Precipitation Hardening*, Elsevier, Amsterdam **1968**.
- [187] H. R. Shercliff, M. F. Ashby, *Acta Metall. Mater.* **1990**, 38, 1789.
- [188] T. Marlaud, A. Deschamps, F. Bley, W. Lefebvre, B. Baroux, *Acta Mater.* **2010**, 58, 248.
- [189] X. Xu, J. Zheng, Z. Li, R. Luo, B. Chen, *Mater. Sci. Eng. A* **2017**, 691, 60.
- [190] K. Wen, Y. Fan, G. Wang, L. Jin, X. Li, Z. Li, Y. Zhang, B. Xiong, *Mater. Des.* **2016**, 101, 16.
- [191] C. Sigli, F. De Geuser, A. Deschamps, J. Lépinoux, M. Perez, C. R. *Phys.* **2018**, 19, 688.
- [192] Q. L. Zhang, K. Ji, O. El Fakir, X. C. Liu, L. L. Wang, *Key Eng. Mater.* **2016**, 716, 402.
- [193] J. Liu, H. Gao, O. El Fakir, L. Wang, J. Lin, in *4th Inter. Conf. on New Forming Technology*, EDP Sciences, Glasgow (UK) **2015**.
- [194] E. Scharifi, *Grundlagen Zur Thermo-Mechanisch Induzierten Eigenschaftsgradierung Von Ausscheidungshärtbaren Aluminiumknetlegierungen*, University of Kassel **2023**.
- [195] E. Scharifi, F. Erbskorn, A. Ademaj, Z. B. Kavaklioglu, U. Weidig and K. Steinhoff, in *Proc. 7th Inter. Conf. Hot Sheet Metal Forming of High Performance Steel*, Wissenschaftliche Scripten, Luleå (SWE) **2019**, 237.
- [196] M. S. Mohamed, A. D. Foster, J. Lin, D. S. Balint, T. A. Dean, *Int. J. Mach. Tools Manuf.* **2012**, 53, 27.
- [197] O. El Fakir, S. Das, I. Stone, G. Scamans, Z. Fan, L. Wang, D. Balint, J. P. Dear, J. Lin, in *Key Engineering Materials*, Trans Tech Publications Ltd, Bäch (CHE), **2014**.
- [198] M. Merklein, M. Wieland, M. Lechner, S. Bruschi, A. Ghiotti, *J. Mater. Process. Technol.* **2016**, 228, 11.
- [199] E. Scharifi, T. Schade, A. Ademaj, S. V. Sajadifar, U. Weidig, T. Niendorf, K. Steinhoff, *Steel Res. Int.* **2021**, 92, 2000633.
- [200] E. Scharifi, M. Roscher, S. Lotz, U. Weidig, E. Jäggle, K. Steinhoff, *Key Eng. Mater.* **2021**, 883, 159.
- [201] E. Scharifi, J. R. Mianroodi, M. Roscher, U. Weidig, E. A. Jäggle, K. Steinhoff, *Mater. Lett.* **2023**, 331, 133465.
- [202] F. Huang, N. R. Tao, *J. Mater. Sci. Technol.* **2011**, 27, 1.
- [203] M. Cabibbo, C. Paoletti, M. Ghat, A. Forcellese, M. Simoncini, *Mater.* **2019**, 12, <https://doi.org/10.3390/ma12091526>.
- [204] S. C. Jacumasso, J. P. de Martins, A. L. M. de Carvalho, *REM Int. Eng. J.* **2016**, 69, 451.
- [205] M. Karlík, P. Homola, M. Slámová, *Characterization Of Aluminium Alloy Sheets Accumulative Roll-Bonded At Different Temperatures*, Canadian Institute of Mining, Metallurgy & Petroleum.
- [206] L. Jiang, J. K. Li, P. M. Cheng, G. Liu, R. H. Wang, B. A. Chen, J. Y. Zhang, J. Sun, M. X. Yang, G. Yang, *Sci. Rep.* **2015**, 4, 3605.
- [207] F. Ostermann, *Anwendungstechnologie Aluminium*, Springer Berlin Heidelberg, Berlin Heidelberg **2014**.
- [208] J.-F. Li, D.-Y. Liu, H. Ning, C. Liu, P.-C. Ma, Y.-L. Chen, X.-H. Zhang, *Mater. Charact.* **2018**, 137, 180.
- [209] F. Roters, D. Raabe, G. Gottstein, *Acta Mater.* **2000**, 48, 4181.



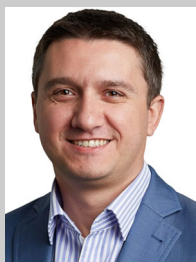
Emad Scharifi completed Ph.D. at University of Kassel (GER) and M.Sc. in Mechanical Engineering, University of Duisburg-Essen (GER). He has done metal forming technology at the Institute of Production Technology and Logistics, University of Kassel (GER). He worked at the Department of Microstructure Physics and Alloy Design, Max-Planck-Institute for Iron Research, Duesseldorf (GER).



Victoria Yardley obtained her M.A., M.Sci. and Ph.D. in materials science and metallurgy from the University of Cambridge (UK). She was formerly senior engineer at Impression Technologies Limited (UK). She currently works as a research associate at Imperial College London (UK) and is director of a technology startup. She is a fellow of the Institute of Sheet Metal Engineering (UK).



Ursula Weidig completed Ph.D. at RWTH Aachen University (GER). She was a research assistant at Department of Metal Forming Technology, Max-Planck-Institute for Iron Research, Duesseldorf (GER). She completed M.Sc. in Materials Engineering from RWTH Aachen University (GER). She is an assistant professor at Metal Forming Technology at the Institute of Production Technology and Logistics, University of Kassel (GER). She has been a chief executive of the Collaborative Research Centre SFB-TRR 30 “Process-integrated manufacturing of functionally graded structures on the basis of thermo-mechanically coupled phenomena,” German Research Foundation DFG (GER). She was a project engineer in research and development in steel and automotive/aerospace/defense industry (CH).



Damian Szegda completed Ph.D. at Brunel University London (UK). He is a research associate, Department of Mechanical Engineering, Brunel University London (UK). He has done his M.Sc. in Mechanical Engineering, Silesian University of Technology (PL). He is the Director of Technology, Impression Technologies Ltd (UK), Chief Computations Officer, Impression Technologies Ltd (UK), and Senior Structural Engineer, Roxel UK Rocket Motors (UK).



Jianguo Lin, FREng, PhD, CEng, FIMechE, FIMMM, works at the Department of Mechanical Engineering, Imperial College London (UK). He completed his Ph.D. at University of Sheffield in 1991. He was a fellow of Institution of Mechanical Engineers (FIMechE, CEng), 2005, and fellow of Institute of Materials, Minerals and Mining (FIMMM), 2011. He is fellow of Royal Academy of Engineering (FREng) 2013, member of European Academy of Science, 2015, chair professor (2008–present) in the Department of Mechanical Engineering, Imperial College London (UK), lecturer (1996–2004), senior lecturer (2004–2006), reader in solid mechanics (2006–2008), University of Birmingham, Department of Mechanical Engineering (UK), and postdoctoral research associate, UMIST (199–1996).



Kurt Steinhoff completed Ph.D. and Habilitation and Venia legendi at RWTH Aachen University (GER). He received a scholarship from Max Planck Society (GER). He was a research assistant, Department of Metal Forming Technology, Max-Planck-Institute for Iron Research, Duesseldorf (GER), and has done his M.Sc. in Mechanical Engineering, University of Duisburg-Essen (GER). He is a full professor of metal forming technology, University of Kassel (GER), has been an associate professor of production technology, Delft University of Technology (NL), has held management positions in production and research and development in steel and automotive/aerospace/defense industry (GER + CH), and is the founder of METAKUS Automotive GmbH (GER).